A DIRECT METHOD FOR BLOCH WAVE EXCITATION BY SCATTERING AT THE EDGE OF A LATTICE. PART II: FINITE SIZE EFFECTS

by R. I. Brougham and I. Thompson

(*Department of Mathematical Sciences,*
University of Liverpool, Liverpool L69 7ZL, UK)

[Received ?? ?? ?? Revise ?? ?? ??]

Summary

A method for determining the reflection and transmission properties of a periodic structure occupying a half-space, previously developed for lattices formed from point scatterers, is generalised to allow for finite size effects. This facilitates the consideration of much higher frequencies (or more precisely, much higher scatterer size to wavelength ratios), and also a wider range of boundary conditions. The method is presented in a general context of linear wave theory, and physical interpretations are given for acoustics, elasticity, electromagnetism and water waves.

1. Introduction

In a recent paper (**1**), the authors developed a new technique for determining the reflection and transmission effects that occur when a wave incident from free space strikes the edge of a periodic structure, such as a crystal. The structure occupies a half-space, so that each row of elements extends to infinity in both directions, but each column is semi-infinite. Applying standard multiple scattering theory (**2**, chapter 4) to this configuration leads to an infinite system of linear, algebraic equations. This system has very poor convergence properties if the parameters are such that Bloch waves are excited inside the lattice. However, using a process called filtering (see (**3**)), the effects of the Bloch waves are 'concentrated' into the first few equations. This results in a rapidly convergent system which can be truncated and solved numerically. The solution can then be used to calculate the amplitudes of all modes that make up the scattered field. In addition, the proportion of incident wave energy that is converted into Bloch waves and transmitted into the lattice is easily determined. This is important in applications where periodic structures are used to guide and control wave propagation (see e.g. (**4**)). For example, band gap filters which limit propagation to certain frequency ranges generally cause some incident wave energy to be lost due to reflection, and the means to predict and minimise these losses is a significant aid to the design process.

The approach taken in (**1**) was to present the method in the simple case of scattering by a semi-infinite lattice of sound-soft (Dirichlet) cylinders in the low frequency limit, where the scatterer radius is asymptotically small relative to the wavelength. A defining feature of such problems is that each lattice element is treated as an isotropic *'point scatterer'*, meaning it is associated with a single radiating mode, with an initially unknown complex amplitude. This choice simplifies the algebra somewhat, but it also restricts the applicability of the technique, both in the range of frequencies that can be considered and also the types of boundary condition. In particular, sound-hard (Neumann) and penetrable bodies cannot be modelled as isotropic point scatterers, even if the frequency of the incident field is very low (**2**, ch. 8). In this sequel paper, the method from (**1**) is generalised to allow

for finite size effects, thereby removing both of these limitations. This extension from the point scatterer case to full linear multiple scattering theory turns out to be remarkably straightforward. Each lattice element is now associated with a series of radiating modes, but the filtering process acts individually on each mode, so that much of the analysis from the point scatterer case carries over directly to the finite size problem. In contrast, an earlier approach to scattering by semi-infinite lattices based on z transforms and the Wiener–Hopf technique, which has been used in several point scatterer problems (**5**, **6**, **7**), is much more difficult to generalise. The analytical obstacles were overcome in (**8**) but the resulting numerical scheme is difficult to implement.

The plan of the paper is as follows. The excitation problem is formulated in section 2, and in section 3 we consider a representation of the field using grating modes. This is central to the evaluation of reflection and transmission coefficients, which in turn are required when calculating the proportion of incident field energy transmitted into the lattice. Some of the results needed in these sections were obtained in (**8**), and we do not repeat their derivations. Before applying the filtering transformation, it is necessary to determine the Bloch vectors for modes that can appear in the far field, deep inside the lattice. Therefore, in section 4, we give brief consideration to the propagation problem where the lattice extends to infinity in all directions and there is no incident wave. The determination of nontrivial solutions to homogeneous problems of this type is a widely studied subject (see (**9**) and (**10**, **11**) for two different approaches to the particular case considered here, and also (**4**) for a range of similar problems and extensive references). A formula for the time-averaged energy flux due to Bloch wave propagation is also obtained in section 4. This is of crucial importance in the excitation problem, since modes that transport energy toward the edge must not be included in the far field. In fact, this is the radiation condition for Bloch wave excitation, without which solutions are nonunique and potentially unphysical. The Sommerfeld condition does not apply inside the lattice, because there is no meaningful concept of phase velocity for Bloch waves (**4**, pp. 40–42). Sections 5 and 6 contain the main theoretical results of the paper. First, the excitation problem is solved using the filtering transformation. The solution is then used to obtain formulae for the reflection and transmission coefficients. Numerical results are presented in section 7 and concluding remarks are made in section 8. There are also two appendices. Some formulas for lattice sums and quasiperiodic Green's functions are given in appendix A. All of these have appeared previously in (**12**) or (**8**), so derivations are omitted. Finally, in appendix B we show that the formula for time-averaged acoustic energy flux derived in (**5**) also applies in electromagnetism, elasticity and water wave theory, with one minor modification.

2. Formulation of the excitation problem

We consider a two-dimensional scattering problem, in which a time-harmonic plane wave is incident upon a semi-infinite lattice formed from circular cylinders of equal radius a. Outside the cylinders, the complex wavefunction $u(\mathbf{r})$ satisfies the Helmholtz equation

$$(\nabla^2 + k^2)u(\mathbf{r}) = 0, \tag{2.1}$$

where k is the wavenumber and $\mathbf{r} = [x, y] \in \mathbb{R}^2$. The construction of the lattice is shown in figure 1. Cylinders are centred at points with position vectors

$$\mathbf{R}_{jp} = j\mathbf{s}_1 + p\mathbf{s}_2, \quad j \in \mathbb{Z}, \quad p = 0, 1, \ldots \tag{2.2}$$

where $\mathbf{s}_1$ and $\mathbf{s}_2$ are basis vectors, which are not parallel to each other, but need not be mutually orthogonal. We may assume without loss of generality that

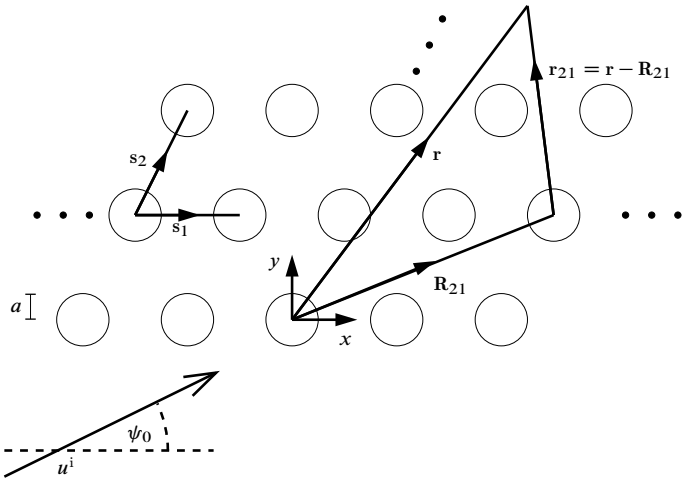

Fig. 1 Schematic diagram showing the lattice, the incident wave and the notation in use.

$$\mathbf{s}_1 = s_1\hat{\mathbf{x}} \quad \text{and} \quad \mathbf{s}_2 = \eta_1\hat{\mathbf{x}} + \eta_2\hat{\mathbf{y}}, \tag{2.3}$$

where the circumflex denotes a unit vector,

$$s_1/2 \geq \eta_1 \geq 0 \quad \text{and} \quad \eta_2 > 0. \tag{2.4}$$

Note the convention that $|\mathbf{v}| = v$ for any vector $\mathbf{v}$, which will be used throughout. A position vector local to the cylinder centred at $\mathbf{r} = \mathbf{R}_{jp}$ is then defined by writing

$$\mathbf{r}_{jp} = \mathbf{r} - \mathbf{R}_{jp}. \tag{2.5}$$

The total field $u^{\mathrm{t}}(\mathbf{r})$ is composed of the incident plane wave

$$u^{\mathrm{i}}(\mathbf{r}) = \mathrm{e}^{\mathrm{i}k(x\cos\psi_0 + y\sin\psi_0)} \tag{2.6}$$

and the scattered field. That is

$$u^{\mathrm{t}}(\mathbf{r}) = u^{\mathrm{i}}(\mathbf{r}) + u^{\mathrm{s}}(\mathbf{r}), \tag{2.7}$$

where $u^{\mathrm{s}}(\mathbf{r})$ is to be determined. Due to the periodicity of the geometry, and of the incident field, u^{s} has a multipole expansion (**2**, ch. 4) of the form

$$u^{\mathrm{s}}(\mathbf{r}) = \sum_{j=-\infty}^{\infty} \mathrm{e}^{\mathrm{i}js_1k\cos\psi_0} \sum_{p=0}^{\infty} \sum_{n=-\infty}^{\infty} A_n^p \mathcal{H}_n(\mathbf{r}_{jp}), \tag{2.8}$$

where $\mathcal{H}_n$ is defined as

$$\mathcal{H}_n(\mathbf{r}) = \mathrm{H}_n^{(1)}(kr)\mathrm{e}^{\mathrm{i}n\theta}. \tag{2.9}$$

Here, $\mathrm{H}_n^{(1)}$ represents a Hankel function of the first kind, and θ is the anticlockwise angle between the x axis and the vector $\mathbf{r}$. The singular wavefunction $\mathcal{H}_n(\mathbf{r})$ satisfies the Helmholtz equation (2.1) (except at $r = 0$), and has the symmetry property

$$\mathcal{H}_n(-\mathbf{r}) = (-1)^n\mathcal{H}_n(\mathbf{r}), \tag{2.10}$$

which is useful later. Note that discarding all wavefunctions except those with order zero in (2.8) and subsequent equations immediately reproduces the analysis from (**1**).

It remains to satisfy the boundary conditions on the cylinder surfaces, and a radiation condition in the limit $y \to \infty$. A system of equations that enforces the boundary conditions was obtained in (**8**), using near-identical notation. There is no need to repeat the derivation here. The result is that

$$A_n^q + Z_n \sum_{m=-\infty}^{\infty} \sum_{p=0}^{\infty} A_m^p S_{m-n}^{q-p}(k\cos\psi_0) = -Z_n \mathrm{i}^n \mathrm{e}^{\mathrm{i}qk(\eta_1\cos\psi_0+\eta_2\sin\psi_0)}\mathrm{e}^{-\mathrm{i}n\psi_0}, \qquad n \in \mathbb{Z}, \quad q = 0, 1, \ldots \tag{2.11}$$

where the function S_n^q is defined as

$$S_n^q(\beta_x) = \begin{cases} \sigma_{-n}(\beta_x) & \text{if } q = 0, \\ G_n(q\mathbf{s}_2; \beta_x) & \text{if } q \neq 0. \end{cases} \tag{2.12}$$

Here, σ_n is the Schlömilch series

$$\sigma_n(\beta_x) = \sum_{j=1}^{\infty} \left[(-1)^n \mathrm{e}^{-\mathrm{i}js_1\beta_x} + \mathrm{e}^{\mathrm{i}js_1\beta_x}\right] \mathrm{H}_n^{(1)}(kjs_1), \tag{2.13}$$

and G_n is the nth order quasiperiodic Green's function for a grating, that is

$$G_n(\mathbf{r}; \beta_x) = \sum_{j=-\infty}^{\infty} \mathrm{e}^{\mathrm{i}js_1\beta_x} \mathcal{H}_n(\mathbf{r} - j\mathbf{s}_1). \tag{2.14}$$

A range of methods for accurately computing σ_n are considered in (**12**). Rapidly convergent representations for G_n, and other quasiperiodic Green's functions used in this article, are given in appendix A. Unlike the Schlömilch series, which (in the context of this work) are simply functions to be computed, the form of the expansion used to evaluate G_n is crucially important to the methods we employ. The scattering coefficients Z_n are determined by the nature of the boundary condition applied on the cylinder surfaces. For the homogeneous Dirichlet condition

$$u^{\mathrm{t}}(\mathbf{r}) = 0 \quad \text{on} \quad r_{jp} = a, \tag{2.15}$$

we have

$$Z_n = \mathrm{J}_n(ka) / \mathrm{H}_n^{(1)}(ka). \tag{2.16}$$

Similarly, for the homogeneous Neumann condition

$$\frac{\partial u^{\mathrm{t}}(\mathbf{r})}{\partial r_{jp}} = 0 \quad \text{on} \quad r_{jp} = a, \tag{2.17}$$

we have

$$Z_n = \mathrm{J}_n'(ka) / \mathrm{H}_n^{(1)\prime}(ka). \tag{2.18}$$

Different scattering coefficients can be used to account for penetrable cylinders (**13**). In a case where no Bloch waves are excited, the system (2.11) can be solved by truncation, because $A_n^p \to 0$ as

$p \to \infty$ and as $|n| \to \infty$. This determines A_n^p, and solves the scattering problem. However, if Bloch waves are excited, then $A_n^p \not\to 0$ as $p \to \infty$, and truncating (2.11) introduces spurious reflection effects from a fictitious upper edge. Developing a means to accurately solve (2.11) in such cases is the main issue to be addressed in the following sections.

The boundary value problem described above can be interpreted in several different physical contexts. In electromagnetism, the wavenumber k is given by

$$k = \omega/c, \tag{2.19}$$

where ω represents frequency and c is the speed of light in the exterior medium. The lattice models a crystalline structure formed from perfectly conducting, infinitely long (in z) cylinders. For transverse magnetic (or s-polarised) waves, the electric field is given by $\mathbf{E} = U(\mathbf{r}; t)\,\hat{\mathbf{z}}$ with

$$U(\mathbf{r}; t) = \mathrm{Re}\big[u(\mathbf{r})\mathrm{e}^{-\mathrm{i}\omega t}\big], \tag{2.20}$$

and a homogeneous Dirichlet boundary condition is applied on the cylinder surfaces. For transverse electric (p-polarised) waves, the magnetic field given by $\mathbf{H} = U(\mathbf{r}; t)\,\hat{\mathbf{z}}$ and a homogeneous Neumann condition is applied on the cylinder surfaces (**2**, §1.4.5). In acoustics, k is again given by (2.19), where now c is the speed of sound in the exterior medium and the potential is given by (2.20). Dirichlet and Neumann boundary conditions model sound-soft and sound-hard cylinders, respectively. The Neumann problem has two further applications. For horizontally polarised shear (SH) waves propagating through an infinite elastic medium with no variation in z, the x- and y-components of displacement are both zero and the z-component is given by (2.20) (**14**, section 7.1). Once again, the wavenumber is given by (2.19), where now c is the shear wave speed (**14**, eqn. (5.1.26)). In linear water wave theory, k is the positive root of the dispersion relation $k \tanh kh = \omega^2/g$, where g is the acceleration due to gravity and h is the fluid depth. In this case, the lattice represents an array of bottom-mounted, surface-penetrating cylinders, and the potential is given by

$$U(\mathbf{r}, z; t) = \mathrm{Re}\big[\phi_0(z)u(\mathbf{r})\mathrm{e}^{-\mathrm{i}\omega t}\big], \tag{2.21}$$

with

$$\phi_0(z) = \frac{g\cosh(kz + kh)}{\mathrm{i}\omega\cosh(kh)}. \tag{2.22}$$

See (**15**, §§1 & 2.4) for details.

3. Grating modes

A series of grating modes of the form

$$u(\mathbf{r}) = \sum_{j=-\infty}^{\infty} \mathrm{e}^{\mathrm{i}\beta_{xj}x}\big[c_j^- \mathrm{e}^{\gamma(\beta_{xj})y} + c_j^+ \mathrm{e}^{-\gamma(\beta_{xj})y}\big], \tag{3.1}$$

where

$$\beta_{xj} = \beta_x + 2j\pi/s_1, \quad j \in \mathbb{Z}, \tag{3.2}$$

and

$$\gamma(t) = \begin{cases} \sqrt{t^2 - k^2} & \text{if } |t| \geq k, \\ -\mathrm{i}\sqrt{k^2 - t^2} & \text{if } |t| < k, \end{cases} \tag{3.3}$$

can be used to represent fields that satisfy the Helmholtz equation (2.1) and the one-dimensional quasiperiodicity condition

$$u(\mathbf{r} + s_1\hat{\mathbf{x}}) = \mathrm{e}^{\mathrm{i}s_1\beta_x}u(\mathbf{r}). \tag{3.4}$$

Since the distinction between propagating modes (for which $\mathrm{Re}[\gamma(\beta_{xj})] = 0$) and evanescent modes (for which $\gamma(\beta_{xj})$ is real and positive) is important, we introduce the sets

$$\mathcal{M} = \big\{j :\ j \in \mathbb{Z},\ |\beta_{xj}| \le k\big\} \quad \text{and} \quad \mathcal{N} = \mathbb{Z} \setminus \mathcal{M}. \tag{3.5}$$

Note that $\mathcal{M}$ is a finite set, which must have at least one entry ($j = 0$) in cases where $|\beta_x| \le k$. It follows from (2.6) that this inequality is always satisfied in problems with plane wave incidence. The number of elements in $\mathcal{M}$ increases with k. To avoid technicalities caused by Wood's anomalies (also sometimes called resonances; see (**16**) for a discussion of different terminologies used), we will assume that $|\beta_{xj}| \neq k$ for any integer j, so that $\gamma(\beta_{xj}) \neq 0$. In other words, we do not attempt to make calculations at the Rayleigh wavelengths for a grating with spacing s_1. The quasiperiodic Green's functions and lattice sums that we use in our subsequent analysis have singularities at these wavelengths. It is possible to remove these singularities from expressions that represent physical fields using the method developed in (**17**), but we have not pursued this. In practice this limitation is very minor because calculations can be made close to a Rayleigh wavelength without any adverse effect.

For the purposes of applying the radiation condition to the far field inside the lattice, and developing a conservation of energy condition, it is useful to determine the rate at which a field of the form (3.1) transports energy across lines parallel to the y axis. Generally, the time-averaged energy flux across a curve $\mathcal{S}$ is given by the line integral

$$\langle E_{\mathcal{S}}\rangle = -\mathsf{C}\,\mathrm{Im}\int_{\mathcal{S}} u(\mathbf{r})\frac{\partial}{\partial n}u^*(\mathbf{r})\,\mathrm{d}s, \tag{3.6}$$

where C is a positive constant that depends on the physical context (see appendix B), the superscript '$*$' denotes a complex conjugate, and the differentiation is in a direction normal to $\mathcal{S}$. If $\langle E_{\mathcal{S}}\rangle > 0$, then the mean flux across $\mathcal{S}$ is in the same direction as the normal. For the particular case of a grating mode expansion, taking $\mathcal{S}$ to be the straight line from $(x_0 - s_1/2, y_0)$ to $(x_0 + s_1/2, y_0)$ and the normal in the direction of increasing y leads to the result

$$\langle E_{\mathcal{S}}\rangle = \mathsf{C}s_1\left[\sum_{j\in\mathcal{M}} |\gamma(\beta_{xj})|\big(|c_j^+|^2 - |c_j^-|^2\big) - 2\sum_{j\in\mathcal{N}} \gamma(\beta_{xj})\,\mathrm{Im}\big[c_j^+(c_j^-)^*\big]\right]. \tag{3.7}$$

See (**1**) or (**8**) for a detailed derivation, and also (**18**) for an earlier appearance of the same formula, in rather different notation.

4. The propagation problem

Before attempting to solve the excitation problem for a semi-infinite lattice, it is necessary to determine the Bloch waves that can be excited in the far field. These are homogeneous solutions to the 'full lattice' problem, in which there is a scatterer centred at $\mathbf{r} = \mathbf{R}_{jp}$ for all integers j and p, and no incident plane wave. Each Bloch wave has a two-dimensional quasiperiodicity property of the form

$$u(\mathbf{r} + \mathbf{R}_{jp}) = \mathrm{e}^{\mathrm{i}\mathbf{R}_{jp}\cdot\boldsymbol{\beta}}u(\mathbf{r}), \tag{4.1}$$

for some Bloch vector

$$\boldsymbol{\beta} = \beta_x \hat{\mathbf{x}} + \beta_y \hat{\mathbf{y}}. \tag{4.2}$$

Note that (4.1) incorporates the one-dimensional condition (3.4). In terms of multipoles, a Bloch wave can be expanded in the form

$$u(\mathbf{r}) = \sum_{n=-\infty}^{\infty} B_n \sum_{j=-\infty}^{\infty} \sum_{p=-\infty}^{\infty} \mathrm{e}^{\mathrm{i}\mathbf{R}_{jp}\cdot\boldsymbol{\beta}} \mathcal{H}_n(\mathbf{r}_{jp}) \tag{4.3}$$

$$= \sum_{n=-\infty}^{\infty} B_n G_n^{(-\infty,\infty)}(\mathbf{r};\boldsymbol{\beta}), \tag{4.4}$$

where $G_n^{(-\infty,\infty)}$ is the nth order quasiperiodic Green's function for the full lattice; see appendix A.

A homogeneous system of equations for the coefficients B_n can be obtained from (4.3) as follows. First, we separate the term with $j = p = 0$ and apply Graf's addition theorem (**2**, thm. 2.12) to expand the other terms about the origin (the notation used in (**2**) is related to the notation used here via $\mathbf{r}_2 = \mathbf{r}_{jp}$ and $\mathbf{r}_1 = \mathbf{r}$, so that $\mathbf{b} = \mathbf{r}_2 - \mathbf{r}_1 = -\mathbf{R}_{jp}$). After using the symmetry property (2.10), we find that

$$u(\mathbf{r}) = \sum_{n=-\infty}^{\infty} B_n \left[\mathrm{H}_n^{(1)}(kr)\mathrm{e}^{\mathrm{i}n\theta} + \sum_{m=-\infty}^{\infty} (-1)^{n+m}\, \Xi_{n-m}(\boldsymbol{\beta})\, \mathrm{J}_m(kr)\mathrm{e}^{\mathrm{i}m\theta} \right], \quad r < \min_{j^2+p^2\neq 0} R_{jp}, \tag{4.5}$$

in which

$$\Xi_n(\boldsymbol{\beta}) = \sum_{j=-\infty}^{\infty} {\sum_{p=-\infty}^{\infty}}' \mathrm{e}^{\mathrm{i}\mathbf{R}_{jp}\cdot\boldsymbol{\beta}} \mathcal{H}_n(\mathbf{R}_{jp}). \tag{4.6}$$

Here, the prime on the summation indicates that the term with $R_{jp} = 0$ is to be omitted. The double series Ξ_n is a two-dimensional lattice sum. A number of methods for evaluating these are discussed in detail in (**12**). One technique which is closely related to the ideas used in this paper is to separate the terms with $p = 0$, which can be written in terms of the Schlömilch series (2.13), and express the remaining terms using quasiperiodic Green's functions. In this way, we find that

$$\Xi_n(\boldsymbol{\beta}) = (-1)^n \left[G_n^{(-\infty,-1)}(\mathbf{0};\boldsymbol{\beta}) + G_n^{(1,\infty)}(\mathbf{0};\boldsymbol{\beta}) \right] + \sigma_n(\beta_x), \tag{4.7}$$

where $G_n^{(-\infty,-1)}$ and $G_n^{(1,\infty)}$ may be evaluated using (A.6) and (A.5), respectively. Returning to (4.5), we apply the boundary condition on $r = a$, multiply by $\mathrm{e}^{-\mathrm{i}p\theta}$ and integrate over one period to obtain

$$B_n + Z_n \sum_{m=-\infty}^{\infty} B_m (-1)^{n+m}\, \Xi_{m-n}(\boldsymbol{\beta}) = 0, \quad n \in \mathbb{Z}, \tag{4.8}$$

with the scattering coefficient Z_n defined in (2.16) or (2.18) for Dirichlet or Neumann boundary coefficients, respectively. In general, the sum Ξ_n and coefficients B_n and Z_n are complex, but a real dispersion relation (which is much easier to solve numerically) can be formed by using the fact that (**12**, §3)

$$\Xi_n(\boldsymbol{\beta}) = -\delta_{n0} + \mathrm{i}\, \Xi_n^{\mathcal{Y}}(\boldsymbol{\beta}), \tag{4.9}$$

where the last term is not necessarily real, but has the symmetry property

$$\Xi_n^{\mathcal{Y}}(\boldsymbol{\beta}) = \left(\Xi_{-n}^{\mathcal{Y}}(\boldsymbol{\beta}) \right)^*. \tag{4.10}$$

In this way, we obtain

$$B_n + W_n \sum_{m=-\infty}^{\infty} B_m (-1)^{n+m} \, \Xi^{\mathcal{Y}}_{m-n}(\boldsymbol{\beta}) = 0, \quad n \in \mathbb{Z}, \tag{4.11}$$

where $W_n = \mathrm{i}Z_n/(1 - Z_n)$ is real. Changing n and m to $-n$ and $-m$, respectively and taking the complex conjugate then shows that $B^*_{-m} = B_m$. A real system can then be formed by writing $B_m = C_m + \mathrm{i}D_m$, $\Xi^{\mathcal{Y}}_m = X_m + \mathrm{i}Y_m$ and taking real and imaginary parts.

The dispersion relation (4.8) is studied in (**9**), for the purpose of identifying the frequency ranges in which nontrivial solutions can exist. Our requirements are slightly different: given fixed values for all other parameters, we must determine the values β_y for which nontrivial solutions can exist. In view of the quasiperiodicity property (4.1), along with (2.3) and (2.2), we need only search within the range $0 \leq \beta_y < 2\pi/\eta_2$. Further details of the process are discussed in (**1**). For each β_y, we can then calculate a vector of coefficients B_n, up to a scalar multiple which plays no role at this point, as we will see. Finally, we seek a grating mode expansion of the form (3.1). Taking $q_0 = q$ and $q_1 = q - 1$, and using the spectral representations (A.5) and (A.6) in (4.4), we find that the amplitude coefficients between rows $q - 1$ and q are given by

$$c_j^+ = \frac{-2\mathrm{i}\mathrm{e}^{qw_j^+}}{s_1 \gamma(\beta_{xj})(\mathrm{e}^{w_j^+} - 1)} \sum_{n=-\infty}^{\infty} B_n \left[\frac{-\mathrm{i}k}{\beta_{xj} + \gamma(\beta_{xj})} \right]^n \tag{4.12}$$

and

$$c_j^- = \frac{-2\mathrm{i}\mathrm{e}^{qw_j^-}}{s_1 \gamma(\beta_{xj})(1 - \mathrm{e}^{w_j^-})} \sum_{n=-\infty}^{\infty} B_n \left[\frac{-\mathrm{i}k}{\beta_{xj} - \gamma(\beta_{xj})} \right]^n, \tag{4.13}$$

where $w_j^\pm$ is defined in (A.4). By using these results in (3.7), we can determine the sign of $\langle E_{\mathcal{S}} \rangle$ for each mode. Modes for which $\langle E_{\mathcal{S}} \rangle > 0$ can be excited by scattering at $y = 0$, but modes for which $\langle E_{\mathcal{S}} \rangle < 0$ carry energy toward the edge, and so must be excluded. This is the radiation condition for the excitation problem. Note that if B_n is replaced by bB_n (i.e. the vector of amplitude coefficients is multiplied by a scalar constant), then $\langle E_{\mathcal{S}} \rangle$ is multiplied by $|b|^2$, so the normalisation of the coefficients has no bearing on this process. Also note that $w_j^\pm$ is pure imaginary for $j \in \mathcal{M}$, and $w_j^+ = (-w_j^-)^*$ for $j \in \mathcal{N}$. Therefore the terms involving q vanish when (4.12) and (4.13) are substituted into (3.7). This happens because Bloch waves propagate through the lattice without loss of energy, meaning that $\langle E_{\mathcal{S}} \rangle$ cannot depend on q.

5. Solution to the excitation problem

Having identified the Bloch waves that can be excited inside the lattice, we are now in a position to solve the linear system (2.11). The main idea that we use is the filtering transformation, which was introduced in (**3**). We begin by decomposing the unknown coefficients A_n^q into decaying contributions and Bloch wave contributions. If the number of Bloch waves excited inside the lattice is λ, and these modes have Bloch vectors $\boldsymbol{\beta}^{(1)}, \ldots, \boldsymbol{\beta}^{(\lambda)}$, then we write

$$A_n^q = \hat{A}_n^q + \sum_{\mu=1}^{\lambda} \mathrm{e}^{\mathrm{i}q\mathbf{s}_2 \cdot \boldsymbol{\beta}^{(\mu)}} B_n^{(\mu)}. \tag{5.1}$$

Here, the coefficients $B_n^{(\mu)}$ must be chosen to satisfy the propagation problem with $\boldsymbol{\beta} = \boldsymbol{\beta}^{(\mu)}$, and each Bloch vector has the same x component, which is inherited from the incident field (2.6). That is

$$\boldsymbol{\beta}^{(\mu)} = \beta_x \hat{\mathbf{x}} + \beta_y^{(\mu)} \hat{\mathbf{y}}, \tag{5.2}$$

with

$$\beta_x = k \cos \psi_0. \tag{5.3}$$

However, solving (4.8) for $B_n^{(\mu)}$ leaves a scalar constant undetermined in each case, representing the amplitude of the corresponding Bloch wave. Determining these amplitudes is the main goal of the filtering procedure. If the correct values are used in (5.1), $\hat{A}_n^q$ will include no contributions from Bloch waves, and so will vanish in the limit $q \to \infty$. Next, we introduce filtered coefficients by writing

$$A_n^{q(\mu)} = \begin{cases} A_n^{q(0)} & \text{if } q = 0 \text{ or } \mu = 0, \\ A_n^{q(\mu-1)} - \mathrm{e}^{\mathrm{i}\mathbf{s}_2 \cdot \boldsymbol{\beta}^{(\mu)}} A_n^{(q-1)(\mu-1)} & \text{otherwise,} \end{cases} \tag{5.4}$$

where $A_n^{q(0)} = A_n^q$ is the original unfiltered coefficient. The idea behind this is that the phase factor $\mathrm{e}^{\mathrm{i}\mathbf{s}_2 \cdot \boldsymbol{\beta}^{(\mu)}}$ causes the contribution from Bloch mode μ to exactly cancel between the two terms on the right-hand side in the last line. This effect can clearly be seen by setting $\mu = 1$ and then substituting the decomposition (5.1) for $A_n^{q(0)}$. In this way, we obtain

$$A_n^{q(1)} = \hat{A}_n^q + \sum_{\mu=1}^{\lambda} \mathrm{e}^{\mathrm{i}q\mathbf{s}_2 \cdot \boldsymbol{\beta}^{(\mu)}} B_n^{(\mu)} - \mathrm{e}^{\mathrm{i}\mathbf{s}_2 \cdot \boldsymbol{\beta}^{(1)}} \left(\hat{A}_n^{q-1} + \sum_{\mu=1}^{\lambda} \mathrm{e}^{\mathrm{i}(q-1)\mathbf{s}_2 \cdot \boldsymbol{\beta}^{(\mu)}} B_n^{(\mu)} \right) \tag{5.5}$$

$$= \hat{A}_n^q - \mathrm{e}^{\mathrm{i}\mathbf{s}_2 \cdot \boldsymbol{\beta}^{(1)}} \hat{A}_n^{q-1} + \sum_{\mu=2}^{\lambda} \mathrm{e}^{\mathrm{i}q\mathbf{s}_2 \cdot \boldsymbol{\beta}^{(\mu)}} B_n^{(\mu)} \left[1 - \mathrm{e}^{\mathrm{i}\eta_2(\beta_y^{(1)} - \beta_y^{(\mu)})} \right]. \tag{5.6}$$

Evidently, the contributions due to the first Bloch wave have been eliminated. We can then apply the transformation a second time to eliminate contributions from the second Bloch mode, etc. After λ applications of (5.4), only the terms involving the decaying coefficients $\hat{A}_n^q$ will remain on the right-hand side, so that $A_n^{q(\lambda)}$ has all Bloch waves removed for $q \geq \lambda$. The expression that arises from this process is complicated, and not directly useful because our aim is to solve (2.11), which is a system of equations for $A_n^{q(0)}$. The important result is that $A_n^{q(\lambda)} \to 0$ as $q \to \infty$. Alongside the fact that the repeated recurrence relation (5.4) can be solved exactly for $A_n^{q(0)}$ this, allows us to transform (2.11) into a rapidly convergent system of equations without any prior knowledge of the Bloch wave amplitudes. The solution to (5.4) is

$$A_n^q = \sum_{\mu=1}^{\lambda} Q_\mu^\lambda \sum_{j=0}^{q} A_n^{j(\lambda)} \mathrm{e}^{\mathrm{i}(q-j)\mathbf{s}_2 \cdot \boldsymbol{\beta}^{(\mu)}}, \tag{5.7}$$

with

$$Q_1^1 = 1 \quad \text{and} \quad Q_\mu^\lambda = \prod_{\substack{\nu=1 \\ \nu \neq \mu}}^{\lambda} \frac{1}{1 - \exp\left[\mathrm{i}\eta_2(\beta_y^{(\nu)} - \beta_y^{(\mu)})\right]}, \quad \lambda > 1. \tag{5.8}$$

Essentially, this result was derived in (**1**); the extra index n which appears here due to the incorporation of finite size effects plays no role at this point because the filtering process acts separately on contributions at each order. Substituting (5.7) into (2.11), we obtain

$$\sum_{\mu=1}^{\lambda} Q_\mu^\lambda \left[\sum_{j=0}^{q} A_n^{j(\lambda)} \mathrm{e}^{\mathrm{i}(q-j)\mathbf{s}_2\cdot\boldsymbol{\beta}^{(\mu)}} + Z_n \sum_{m=-\infty}^{\infty} \sum_{p=0}^{\infty} \sum_{j=0}^{p} A_m^{j(\lambda)} \mathrm{e}^{\mathrm{i}(p-j)\mathbf{s}_2\cdot\boldsymbol{\beta}^{(\mu)}} S_{m-n}^{q-p}(k\cos\psi_0) \right] = -Z_n \mathrm{i}^n \mathrm{e}^{\mathrm{i}qk(\eta_1\cos\psi_0+\eta_2\sin\psi_0)} \mathrm{e}^{-\mathrm{i}n\psi_0}, \quad n\in\mathbb{Z}, \quad q=0,1,\ldots \tag{5.9}$$

Now (5.9) cannot be solved by truncation in its current form, because terms with large p involve $A_m^{0(\lambda)}, A_m^{1(\lambda)}, \ldots$ However, after interchanging the summations over p and j, the innermost sum can be evaluated using (2.12) and (A.2). In this way, we find that

$$\sum_{\mu=1}^{\lambda} Q_\mu^\lambda \left[\sum_{j=0}^{q} A_n^{j(\lambda)} \mathrm{e}^{\mathrm{i}(q-j)\mathbf{s}_2\cdot\boldsymbol{\beta}^{(\mu)}} + Z_n \sum_{m=-\infty}^{\infty} \sum_{j=0}^{\infty} A_m^{j(\lambda)} \mathrm{e}^{\mathrm{i}(q-j)\mathbf{s}_2\cdot\boldsymbol{\beta}^{(\mu)}} \Gamma_{m-n}^{j-q}(\boldsymbol{\beta}^{(\mu)}) \right] = -Z_n \mathrm{i}^n \mathrm{e}^{\mathrm{i}qk(\eta_1\cos\psi_0+\eta_2\sin\psi_0)} \mathrm{e}^{-\mathrm{i}n\psi_0}, \quad n\in\mathbb{Z}, \quad q=0,1,\ldots \tag{5.10}$$

where

$$\Gamma_n^q(\boldsymbol{\beta}) = \begin{cases} G_n^{(q,\infty)}(\mathbf{0};\boldsymbol{\beta}) & \text{if } q>0, \\ G_n^{(1,\infty)}(\mathbf{0};\boldsymbol{\beta}) + \sigma_{-n}(\beta_x) & \text{if } q=0, \\ G_n^{(q,-1)}(\mathbf{0};\boldsymbol{\beta}) + \sigma_{-n}(\beta_x) + G_n^{(1,\infty)}(\mathbf{0};\boldsymbol{\beta}) & \text{if } q<0. \end{cases} \tag{5.11}$$

Note that Γ_n^q is closely related to the lattice sum Ξ_n defined in equation (4.6), but with rows $q-1, q-2, \ldots$ omitted; in fact $\Gamma_n^{-\infty}(\boldsymbol{\beta}) = (-1)^n\,\Xi_n(\boldsymbol{\beta})$. Once computed, solutions to (5.10) can be verified using infinite array subtraction. The procedure is very similar to the case of point scatterers (**1**), so we need not repeat the details here.

Finally, we obtain the coefficients for the excited Bloch waves by equating (5.1) to (5.7) and setting $q=P$, say, with P chosen so that $\hat{A}_n^q$ is negligible for $q\geq P$. In this way, we find that

$$\sum_{\mu=1}^{\lambda} B_n^{(\mu)} \mathrm{e}^{\mathrm{i}P\mathbf{s}_2\cdot\boldsymbol{\beta}^{(\mu)}} = \sum_{\mu=1}^{\lambda} \left(Q_\mu^\lambda \sum_{j=0}^{P} A_n^{j(\lambda)} \mathrm{e}^{-\mathrm{i}j\mathbf{s}_2\cdot\boldsymbol{\beta}^{(\mu)}} \right) \mathrm{e}^{\mathrm{i}P\mathbf{s}_2\cdot\boldsymbol{\beta}^{(\mu)}}, \tag{5.12}$$

and we can now simply read off the Bloch wave coefficients as

$$B_n^{(\mu)} = Q_\mu^\lambda \sum_{j=0}^{P} A_n^{j(\lambda)} \mathrm{e}^{-\mathrm{i}j\mathbf{s}_2\cdot\boldsymbol{\beta}^{(\mu)}}. \tag{5.13}$$

An alternative way to derive (5.13) is to repeatedly apply filtering to (5.1) using (5.4) to obtain an expression for $A_n^{q(\lambda-1)}$. This coefficient includes a contribution from only one Bloch wave. The effect of a single filtering is shown in (5.6). The pattern exhibited by the Bloch wave contributions is straightforward: each successive application eliminates one term from the lower end of the series, $\mu=\nu$, say, and introduces a factor $1-\mathrm{e}^{\mathrm{i}\eta_2(\beta_y^{(\nu)}-\beta_y^{(\mu)})}$ to the others. The product of all such factors up to $\nu=\lambda-1$ is $1/Q_\lambda^\lambda$, defined in (5.8). Therefore, by filtering $\lambda-1$ times, we find that

$$A_n^{q(\lambda-1)} = \langle\text{decaying terms}\rangle + \mathrm{e}^{\mathrm{i}q\mathbf{s}_2\cdot\boldsymbol{\beta}^{(\lambda)}} \frac{B_n^{(\lambda)}}{Q_\lambda^\lambda}. \tag{5.14}$$

A second expression for $A_n^{q(\lambda-1)}$ can be obtained by solving one level of the repeated recurrence relation (5.4) to obtain

$$A_n^{q(\lambda-1)} = \sum_{j=0}^{q} A_n^{j(\lambda)} \mathrm{e}^{\mathrm{i}(q-j)\mathbf{s}_2\cdot\boldsymbol{\beta}^{(\lambda)}}. \tag{5.15}$$

Equating this to (5.14), and taking the limit $q \to \infty$, we find that

$$B_n^{(\lambda)} = Q_\lambda^\lambda \sum_{j=0}^{\infty} A_n^{j(\lambda)} \mathrm{e}^{-\mathrm{i}j\mathbf{s}_2\cdot\boldsymbol{\beta}^{(\lambda)}}. \tag{5.16}$$

Finally, we observe that (5.7) is not affected if the Bloch wave vectors $\boldsymbol{\beta}^{(1)}, \ldots, \boldsymbol{\beta}^{(\lambda)}$ and their associated Q coefficients are rearranged, so in fact (5.16) holds for all Bloch waves, not just the last. This gives us (5.13) with P replaced by ∞, which is formally correct. Note that the upper index on Q, and the bracketed index on A refer to the number of Bloch waves that can be excited, and so these do not change when the ordering of the Bloch wave vectors is changed. Each set of coefficients $B_n^{(\mu)}$ calculated using (5.13) or (5.16) forms a particular solution to the propagation problem (see section 4) with $\boldsymbol{\beta} = \boldsymbol{\beta}^{(\mu)}$ and the scaling set so that $\hat{A}_n^q \to 0$ in (5.1). The scaling constants cannot be determined from the propagation problem.

6. Reflection and transmission

In the region where $y < 0$, and between each consecutive pair of rows, the field can be represented as an expansion in grating modes of the form (3.1). That is,

$$u(\mathbf{r}) = \sum_{j=-\infty}^{\infty} \mathrm{e}^{\mathrm{i}kx\cos\psi_j}\left[c_{jq}^{-}\mathrm{e}^{-\mathrm{i}ky\sin\psi_j} + c_{jq}^{+}\mathrm{e}^{\mathrm{i}ky\sin\psi_j}\right], \quad \begin{cases} (q-1)\eta_2 < y < q\eta_2, & \text{if } q \in \mathbb{N}, \\ 0 < y, & \text{if } q = 0. \end{cases} \tag{6.1}$$

Here, the scattering angles ψ_j are defined via

$$k\cos\psi_j = k\cos\psi_0 + 2j\pi/s_1 \quad \text{and} \quad k\sin\psi_j = \mathrm{i}\gamma(k\cos\psi_j), \tag{6.2}$$

with γ defined by (3.3). Note that $\cos\psi_j$ is always real, whereas $\sin\psi_j$ may be positive real or positive imaginary (but not zero since we are not calculating the field at Rayleigh wavelengths; see section 3). The process of obtaining the amplitude coefficients $c_{jq}^{\pm}$ is very similar to the point scatterer case (**1**), so we present only a summary here.

For $y < 0$, there is only one upwards oriented mode, which is the incident field (2.6). Therefore $c_{00}^{+} = 1$, and $c_{j0}^{+} = 0$ for $j \neq 0$. The reflected field consists of a set of downwards oriented grating modes, exactly as it does for a single periodic grating (**19**, **20**). To determine their amplitudes, we substitute (5.1) into (2.8) and then use (2.14) and (A.2) to obtain

$$u^{\mathrm{s}}(\mathbf{r}) = \sum_{n=-\infty}^{\infty}\left[\sum_{\mu=1}^{\lambda} B_n^{(\mu)} G_n^{(0,\infty)}(\mathbf{r};\boldsymbol{\beta}^{(\mu)}) + \sum_{p=0}^{\infty} \hat{A}_n^p G_n(\mathbf{r} - p\mathbf{s}_2;\beta_x)\right]. \tag{6.3}$$

Next, we use the spectral forms of the quasiperiodic Green's functions (A.7) and (A.10), and in this way we find that

$$c_{j0}^{-} = \frac{2}{ks_1\sin\psi_j}\sum_{n=-\infty}^{\infty}(-\mathrm{i})^n\mathrm{e}^{-\mathrm{i}n\psi_j}\left[\sum_{\mu=1}^{\lambda}\frac{B_n^{(\mu)}\tau_j}{\tau_j - \mathrm{e}^{\mathrm{i}\mathbf{s}_2\cdot\boldsymbol{\beta}^{(\mu)}}} + \sum_{p=0}^{\infty}\hat{A}_n^p\tau_j^{-p}\right], \tag{6.4}$$

where τ_j is given by (A.9). The coefficients c^-_{j0} describe the response of the semi-infinite lattice to excitation by an arbitrary plane wave; they can be used to form the reflection scattering matrix, often referred to as $\mathbf{R}_\infty$ (**21**).

To determine the transmitted field, we begin by decomposing the total field into two terms; thus

$$u^{\mathrm{t}}(\mathbf{r}) = \hat{u}^{\mathrm{t}}(\mathbf{r}) + u^{\mathrm{b}}(\mathbf{r}), \tag{6.5}$$

with

$$\hat{u}^{\mathrm{t}}(\mathbf{r}) = \mathrm{e}^{\mathrm{i}k(x\cos\psi_0 + y\sin\psi_0)} + \sum_{n=-\infty}^{\infty}\Bigg[\sum_{p=0}^{\infty}\hat{A}_n^p G_n(\mathbf{r} - p\mathbf{s}_2;\beta_x) - \sum_{\mu=1}^{\lambda} B_n^{(\mu)} G_n^{(-\infty,-1)}\big(\mathbf{r};\boldsymbol{\beta}^{(\mu)}\big)\Bigg] \tag{6.6}$$

and

$$u^{\mathrm{b}}(\mathbf{r}) = \sum_{n=-\infty}^{\infty}\sum_{\mu=1}^{\lambda} B_n^{(\mu)} G_n^{(-\infty,\infty)}\big(\mathbf{r};\boldsymbol{\beta}^{(\mu)}\big). \tag{6.7}$$

The idea here is that, since the far field inside the lattice consists of Bloch waves alone, contributions from $\hat{u}^{\mathrm{t}}$ must vanish as $y \to \infty$. Now if we write

$$c^{\pm}_{jq} = \hat{c}^{\pm}_{jq} + b^{\pm}_{jq}, \tag{6.8}$$

where the terms on the right-hand side are the contributions from (6.6) and (6.7), respectively, then (A.11) with $q_1 = q - 1$ and (A.10) with $q_0 = q$ immediately yield

$$b^+_{jq} = \frac{2\rho_j^q}{ks_1\sin\psi_j}\sum_{n=-\infty}^{\infty}(-\mathrm{i})^n\mathrm{e}^{\mathrm{i}n\psi_j}\sum_{\mu=1}^{\lambda}\frac{\mathrm{e}^{\mathrm{i}q\mathbf{s}_2\cdot\boldsymbol{\beta}^{(\mu)}}B_n^{(\mu)}}{\rho_j\mathrm{e}^{\mathrm{i}\mathbf{s}_2\cdot\boldsymbol{\beta}^{(\mu)}} - 1} \tag{6.9}$$

and

$$b^-_{jq} = \frac{2\tau_j^{1-q}}{ks_1\sin\psi_j}\sum_{n=-\infty}^{\infty}(-\mathrm{i})^n\mathrm{e}^{-\mathrm{i}n\psi_j}\sum_{\mu=1}^{\lambda}\frac{\mathrm{e}^{\mathrm{i}q\mathbf{s}_2\cdot\boldsymbol{\beta}^{(\mu)}}B_n^{(\mu)}}{\tau_j - \mathrm{e}^{\mathrm{i}\mathbf{s}_2\cdot\boldsymbol{\beta}^{(\mu)}}}. \tag{6.10}$$

For $\hat{c}^-_{jq}$, we observe that only the central term on the right-hand side of (6.6) includes downward-oriented modes, and using (A.7) shows that

$$\hat{c}^-_{jq} = \frac{2\tau_j^{-q}}{ks_1\sin\psi_j}\sum_{n=-\infty}^{\infty}(-\mathrm{i})^n\mathrm{e}^{-\mathrm{i}n\psi_j}\sum_{p=0}^{\infty}\hat{A}_n^{p+q}\tau_j^{-p}. \tag{6.11}$$

Finally, for $\hat{c}^+_{jq}$, we find that

$$\hat{c}^+_{jq} = \delta_{j0} + \frac{2}{ks_1\sin\psi_j}\sum_{n=-\infty}^{\infty}(-\mathrm{i})^n\mathrm{e}^{\mathrm{i}n\psi_j}\left[\sum_{p=0}^{q-1}\hat{A}_n^p\rho_j^p + \sum_{\mu=1}^{\lambda}\frac{B_n^{(\mu)}}{1-\rho_j\mathrm{e}^{\mathrm{i}\mathbf{s}_2\cdot\boldsymbol{\beta}^{(\mu)}}}\right]. \tag{6.12}$$

For the case of point scatterers, it is shown in (**1**) that contributions from modes with amplitudes $\hat{c}^-_{jq}$ and $\hat{c}^+_{jq}$ disappear in the far field: the former for all j, and the latter for $j \in \mathcal{N}$ (see (3.5)). The arguments required are not affected by the presence of the sum over n that appears in finite size case,

so there is no need to repeat them here. On the other hand, it has not been possible show analytically that propagating modes with amplitudes $\hat{c}_{jq}^{+}$ are not present in the far field. A proof is given in (**8**), but there the entire problem is approached in a rather different way, and the proof does not appear to correspond to any argument that can be based on the analysis used in this paper. However, we can use the fact that the far field must consist entirely of Bloch waves to conclude that

$$\delta_{j0} + \frac{2}{ks_1 \sin\psi_j} \sum_{n=-\infty}^{\infty} (-\mathrm{i})^n \mathrm{e}^{\mathrm{i}n\psi_j} \left[\sum_{p=0}^{\infty} \hat{A}_n^p \rho_j^p + \sum_{\mu=1}^{\lambda} \frac{B_n^{(\mu)}}{1 - \rho_j \mathrm{e}^{\mathrm{i}\mathbf{s}_2 \cdot \boldsymbol{\beta}^{(\mu)}}} \right] = 0, \quad j \in \mathcal{M}. \tag{6.13}$$

We can also derive a conservation of energy condition using grating mode expansions. Again, this is very similar to the point scatterer case considered in (**1**). We evaluate the integral (3.6), taking $\mathcal{S}$ to be the parallelogram with vertices at

$$\mathbf{r} = \pm \tfrac{1}{2}\mathbf{s}_1 \pm (P - \tfrac{1}{2})\mathbf{s}_2, \quad P = 1, 2, \ldots \tag{6.14}$$

and differentiating in the direction of the outgoing normal to each edge. The contributions from the sides parallel to $\mathbf{s}_2$ cancel each other, due to the one-dimensional quasiperiodicity property (3.4). For the edge beneath the lattice, we substitute $c_{j0}^{\pm}$ from (6.4) for $c_j^{\pm}$ in (3.7). Using the fact that $c_{j0}^{+} = \delta_{j0}$, and taking into account the orientation of the outgoing normal (which introduces a factor -1), we find that the time averaged energy flux across this line is

$$E_1 = -ks_1 \mathsf{C} \left[\sin\psi_0 - \sum_{j \in \mathcal{M}} \sin\psi_j |c_{j0}^{-}|^2 \right]. \tag{6.15}$$

Thus, all of the plane waves present in the region $y < 0$ (but not the evanescent modes) contribute to the energy flux across the lower edge of $\mathcal{S}$. If no Bloch waves are excited insider the lattice, then all of the incident energy must be reflected back, so we must have $E_1 = 0$. If Bloch waves are excited, then the average energy flux across the lower edge of $\mathcal{S}$ is in the direction of the *inward* normal (some incident wave energy is transmitted into the lattice, so less is reflected back). In this case $E_1 < 0$ and

$$E_1 + E_2 = 0, \tag{6.16}$$

where E_2 is the time averaged energy flux across the upper edge of the parallelogram. To calculate this, we replace $c_j^{\pm}$ in (3.7) with $b_{jP}^{\pm}$, given by (6.9) and (6.10). If $\lambda = 1$, so that a single Bloch wave is excited, straightforward algebra shows that $|b_{jP}^{\pm}|$ and $b_{jP}^{+}(b_{jP}^{-})^*$ are independent of P, for $j \in \mathcal{M}$ and for $j \in \mathcal{N}$, respectively. Therefore we may set $P = 0$ before substituting into (3.7). If $\lambda > 1$ these simplifications no longer occur, but E_2 cannot depend on P because Bloch waves propagate through the lattice without loss of energy. A simple proof that we may still use $b_{j0}^{\pm}$ to calculate E_2 can be achieved by applying Green's second identity to a field u and its complex conjugate, on the region bounded by the parallelogram $\widehat{\mathcal{S}}$, which has vertices at $\mathbf{r} = \pm\frac{1}{2}\mathbf{s}_1 - \frac{1}{2}\mathbf{s}_2$ and $\mathbf{r} = \pm\frac{1}{2}\mathbf{s}_1 + (P - \frac{1}{2})\mathbf{s}_2$ for any integer P, excluding the interior of any scatterers this contains. Using the fact that $\nabla^2 u = -k^2 u$, and similarly for u^*, Green's identity immediately reduces to

$$\mathrm{Im} \int_{\widehat{\mathcal{S}}} u(\mathbf{r}) \frac{\partial}{\partial n} u^*(\mathbf{r}) \, \mathrm{d}s = 0. \tag{6.17}$$

Contributions from the surfaces of the scatterers are all zero, because there either $u = 0$ or $\partial u/\partial n =$

0, due to the boundary conditions. Now if u consists of multiple Bloch waves, each with the same value for β_x, then contributions from the edges parallel to $\mathbf{s}_2$ cancel, due to the quasiperiodicity condition (3.4). Hence, the contributions from the upper and lower edges are equal, except for a factor -1, which comes from the different orientations of the outgoing normals.

Finally, we observe that the first term on the right-hand side of (6.15) is due to the incident wave, whereas the sum is due to the reflected field. Thus, if we divide by $ks_1\mathsf{C}\sin\psi_0$, we obtain the proportion of incident energy that is reflected back from the lattice,

$$E_R = \frac{1}{\sin\psi_0}\sum_{j\in\mathcal{M}}\sin\psi_j|c_{j0}^-|^2. \tag{6.18}$$

This important quantity is used extensively in the next section.

7. Numerical results

The method described in the preceding sections has been implemented in Fortran 2003. The indices n and m in (5.10), which denote the modes used in the expansion of the field about each scatterer (see (2.8)) and the indices j and q, which denote the rows retained in the filtered system, are truncated by automated processes.

Generally, sums over mode indices converge very rapidly, though more terms are needed for larger values of ka. The truncation parameter for these sums is determined using the coefficients Z_n defined in (2.16) and (2.18). We find the largest value in the sequence $|Z_0|, |Z_1|, \ldots$ and denote this by $Z_{\max}$. Next we find the smallest natural number N such that

$$|Z_{N+j}| < \delta\, Z_{\max}, \quad j = 0, 1, \ldots \tag{7.1}$$

where δ is a tolerance parameter which we typically set at 10^{-8}. Terms with $|n| < N$ are retained, and the others are discarded. Note that it is not sufficient to inspect the single ratio $|Z_N|/Z_{\max}$, because it may be that $Z_N \approx 0$ for a particular n if ka is close to a zero of $\mathrm{J}_N(ka)$ or $\mathrm{J}'_N(ka)$, and this is unrelated to the fact that $Z_n \to 0$ as $n \to \infty$.

To determine the number of rows needed, we first observe that the field inside the lattice may be viewed as consisting of Bloch waves and evanescent modes for which $\mathrm{Im}[\beta_y] > 0$. The rate of decay of these evanescent modes determines the rate at which the filtered system (5.10) converges. We aim to choose a truncation parameter P so that

$$\big\|A_n^{P(\lambda)}\big\|_2 < \delta\big\|A_n^{0(\lambda)}\big\|_2, \tag{7.2}$$

where $\|\cdot\|_2$ represents a Euclidean norm, summing over n with the upper indices fixed. Initially, we truncate and solve the system, retaining rows $0, \ldots, P_0$, say. Should this fail to achieve the required accuracy, the number of additional rows needed is estimated by reasoning as follows. Since the fully filtered coefficients $A_n^{q(\lambda)}$ do not include contributions from the Bloch waves if $q \geq \lambda$ (see §5), we may obtain the approximate rate of exponential decay by comparing the norms of the vectors $A_n^{\lambda(\lambda)}$ and $A_n^{P_0(\lambda)}$. Thus, if we assume that

$$\big\|A_n^{p+1(\lambda)}\big\|_2 \approx \mathrm{e}^{-\alpha}\big\|A_n^{p(\lambda)}\big\|_2 \tag{7.3}$$

for $p \geq \lambda$ then

$$\alpha \approx \frac{1}{\lambda - P_0}\ln\frac{\big\|A_n^{P_0(\lambda)}\big\|_2}{\big\|A_n^{\lambda(\lambda)}\big\|_2}. \tag{7.4}$$

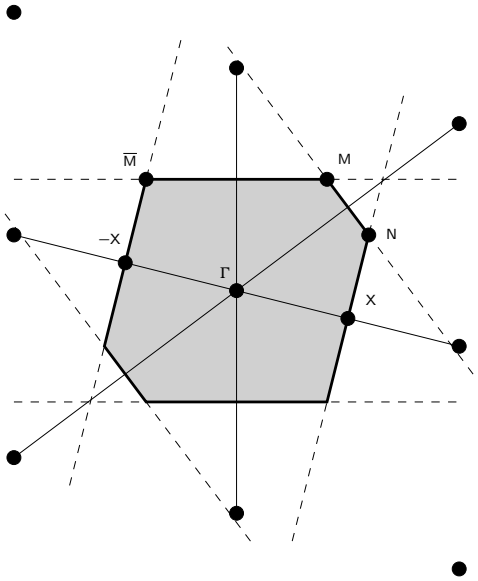

Fig. 2 The Brillouin zone for an arbitrary, skewed lattice. The shaded region is the full Brillouin zone, and the pentagon $\mathsf{X}(-\mathsf{X})\overline{\mathsf{M}}\mathsf{MN}\mathsf{X}$ is the irreducible zone. Points below the line $\mathsf{X}(-\mathsf{X})$ are excluded from the irreducible zone due to 180° rotational symmetry. The point Γ (the origin) is a vertex of the irreducible zone in certain cases with additional symmetries.

The estimate for P is then given by

$$P = \lambda + \left\lceil \frac{-\ln \delta}{\alpha} \right\rceil, \tag{7.5}$$

where $\lceil \cdot \rceil$ means round toward infinity. A small value for P_0 allows results for cases in which the convergence is rapid to be computed very efficiently. A larger value leads to unnecessary calculations in many cases, but also increases the range of parameters for which (7.2) is achieved immediately, without the need to recalculate with P given by (7.5). We find that $P_0 = 15$ gives a good compromise between these factors. For some parameter sets, an evanescent mode with $\mathrm{Im}[\beta_y] \ll 1$ is excited, and it is not practical to achieve (7.2). If the number of rows estimated by (7.5) is greater than 150, then we simply calculate E_R given by (6.18) for successively increased truncation parameters P. Since E_R is the final result plotted in the reflection diagrams shown below (as opposed to an intermediate value used in later calculations), we accept values that have converged to four significant figures. Occasionally the program encountered a situation in which the value of E_R does not converge. This occurs in cases where the rate of decay of one or more evanescent modes is exceptionally low. Such convergence failures are rare, accounting for 0.025%, 0.14%, 0.012% and 0.49% of the data in figures 3–7, respectively. The images are corrected by averaging the values of E_R at surrounding points.

We now present some figures that illustrate the results that can be obtained using our method. In each case, we include a standard band diagram, alongside a *reflection diagram*. Band diagrams are obtained by solving the propagation problem. These have the wavenumber k on the vertical axis,

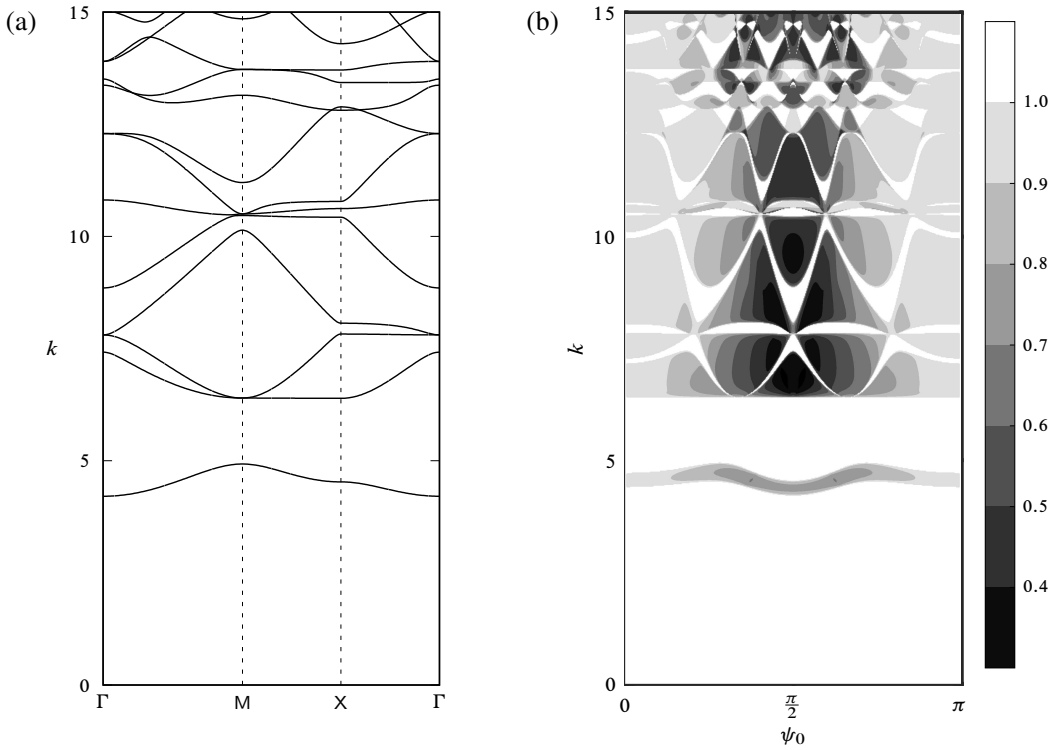

Fig. 3 Band diagram (a) and reflection diagram (b) for a lattice of Dirichlet scatterers with radius $a = 0.26$ and basis vectors $\mathbf{s}_1 = [1, 0]$ and $\mathbf{s}_2 = [0, 1]$.

and the variable on the horizontal axis represents a location on the edge of the irreducible Brillouin zone. The Brillouin zone is the region of two-dimensional space which contains the shortest possible representation for each Bloch vector, accounting for the quasiperiodicity property (4.1). This can then be further reduced using symmetry to obtain the irreducible Brillouin zone (see (**4**, Appendix B) for details). In the most general case, the Brillouin zone is an irregular hexagon, as shown in figure 2. The presence of 180° rotational symmetry in the propagation problem means it is only necessary to consider one half of this hexagon (all possible modes can be described by a Bloch vector located on or above the line from $-\mathsf{X}$ to X) in figure 2). The coordinates of the vertices are then given by (**22**)

$$\mathsf{X} = \frac{\pi}{s_1}\left(1, -\frac{\eta_1}{\eta_2}\right), \quad \mathsf{M} = \frac{\pi}{\eta_2^2}\left(\frac{\eta_1^2+\eta_2^2}{s_1} - \eta_1, \eta_2\right), \quad \mathsf{N} = \frac{\pi}{\eta_2^2}\left(\eta_1 + \frac{\eta_2^2-\eta_1^2}{s_1}, \eta_2\left(1 - \frac{2\eta_1}{s_1}\right)\right), \tag{7.6}$$

with $\overline{\mathsf{M}}$ representing the reflection of the point M through the vertical axis. The minimum and maximum frequency for each Bloch mode occur when its Bloch vector $\boldsymbol{\beta}$ lies on the edge of the irreducible Brillouin zone, so plotting against k shows the locations of the band gaps. Reflection diagrams are obtained by solving the excitation problem. These also have k on the vertical axis, but the variable on the horizontal axis is now the angle of incidence ψ_0, which is related to the Bloch vectors for the excited modes via (5.3). The shading indicates the proportion of incident energy

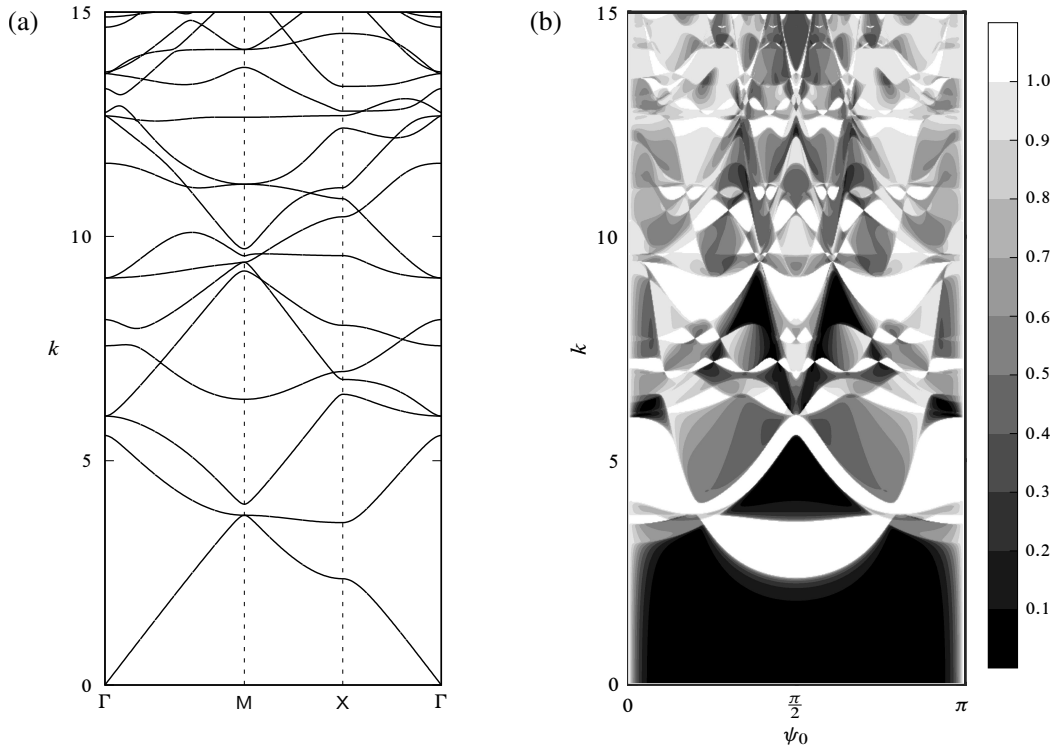

Fig. 4 Band diagram (a) and reflection diagram (b) for a lattice of Neumann scatterers with radius $a = 0.26$ and basis vectors $\mathbf{s}_1 = [1, 0]$ and $\mathbf{s}_2 = [0, 1]$.

reflected back from the lattice, calculated using (6.18). Unshaded regions correspond to parameter regimes in which all energy is reflected, whereas darker shading indicates higher transmission.

Figures 3–5 show results for square lattices, with $\mathbf{s}_1 = [1, 0]$ and $\mathbf{s}_2 = [0, 1]$. Since these basis vectors are mutually orthogonal, it is easy to deduce that the irreducible Brillouin zone for this case is a triangle, with vertices at the points

$$\Gamma = (0, 0), \quad \mathsf{M} = (\pi, \pi) \quad \text{and} \quad \mathsf{X} = (\pi, 0). \tag{7.7}$$

Band diagrams for the same parameters can also be found in (**9**), and our results are clearly in agreement (note however that the vertices of the irreducible Brillouin zone are ordered differently in (**9**); we follow (**4**) in placing Γ at the edges of the plots, since the origin appears on the boundary of the zone for all lattice types).

Figure 3 shows the band diagram (a) and reflection diagram (b) for cylinders with radius $a = 0.26$ and Dirichlet boundary conditions imposed on the surface. There is a band gap for $k \lessapprox 4.21$, where no modes can propagate. This 'low frequency gap' is a characteristic property of lattices formed from Dirichlet scatterers (see (**9**) for details). There is then a second gap for $4.93 \lessapprox k \lessapprox 6.39$, and above this the diagram becomes very complicated, with an increasing number of modes present at higher frequencies. The same facts concerning gaps can be obtained from the reflection diagram, but this also contains significant information about the behaviour of the field within pass bands. For the

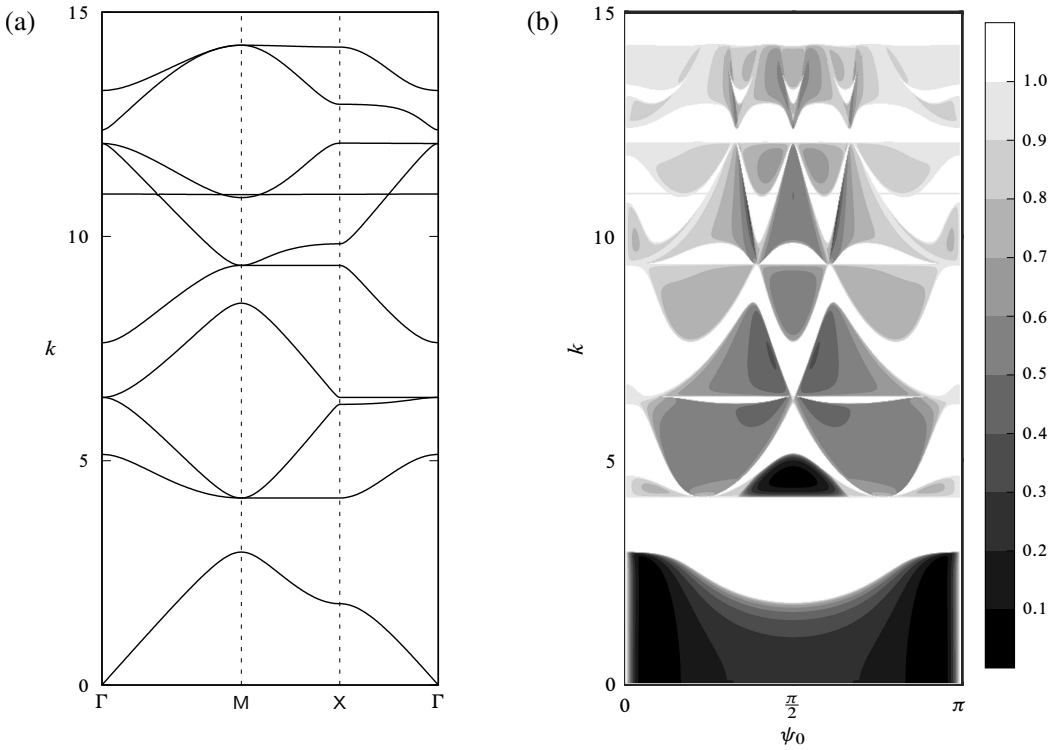

Fig. 5 Band diagram (a) and reflection diagram (b) for a lattice of Neumann scatterers with radius $a = 0.42$ and basis vectors $\mathbf{s}_1 = [1, 0]$ and $\mathbf{s}_2 = [0, 1]$.

narrow band between $k \approx 4.21$ and $k \approx 4.93$, there is relatively little transmission, and most of the incident energy is reflected back from the lattice. On the other hand, above the second gap there are some regions of very high transmission, particularly around head-on incidence ($\psi_0 = \pi/2$).

The parameters used in in figure 4 are the same as those in figure 3, except that Neumann conditions are now imposed on the cylinder surfaces. In general, Neumann conditions lead to greater transmission and so the contours used to shade figure 4(b) (and subsequent reflection diagrams) are slightly different to those in figure 3. There are no band gaps in figure 4, but again the pattern is relatively simple at low frequencies, and much more complicated at higher frequencies, where there are many more modes. The reflection diagram also captures this information, and in addition shows that in place of the low frequency gap there is a regime in which over 90% of the incident wave energy is transmitted into the lattice. This region covers all angles of incidence except grazing for $k \lessapprox 2$, and persists to $k \approx 3$ for $\psi_0 \approx \pi/4$ and $\psi_0 \approx 3\pi/4$. Above the high transmission region, there are significant partial band gaps, in which total reflection occurs, but only for certain angles of incidence. At higher frequencies, the pattern again becomes increasingly complex, though some notable features include another region of very high transmission for $4 \lessapprox k \lessapprox 5$ and $\psi_0 \approx \pi/2$, and three further partial band gaps for $7.5 \lessapprox k \lessapprox 9.5$. Above these regions, there is relatively little transmission.

Figure 5 shows results for a more concentrated lattice, with cylinder radius $a = 0.42$, and Neumann

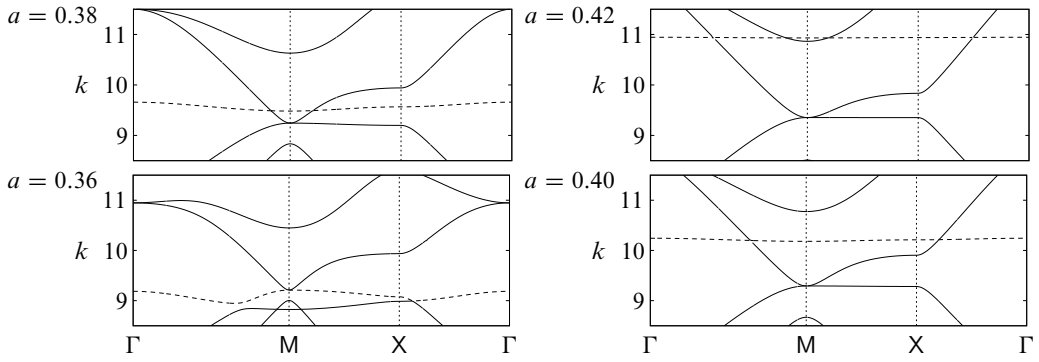

Fig. 6 Sections of the band diagram for a square lattice with $\mathbf{s}_1 = [1, 0]$ and $\mathbf{s}_2 = [0, 1]$. Neumann boundary conditions are enforced on the cylinder surfaces.

boundary conditions in force on the surfaces. Increasing the scatterer radius causes a total band gap to appear between $k \approx 2.96$ and $k \approx 4.17$. In addition, the regions of high transmission are significantly reduced in size, and for $k \gtrapprox 4.17$ there are many partial band gaps, and many small parameter regimes in which some transmission is possible, though most of the incident energy is reflected back. A second total band gap has appeared for $12.1 \lessapprox k \lessapprox 12.4$, and a third occurs for $k \gtrapprox 14.3$. The upper limit for the third gap is outside the range of the plot; it persists up to $k \approx 15.2$. The corresponding results for Dirichlet boundary conditions show modes existing in very narrow frequency ranges and little to no transmission for any combination of ψ_0 and k, and therefore these are not shown. An unusual feature of the band diagram in figure 5(b) is the very 'flat' mode at $k \approx 10.9$. The effect of this mode is also visible in the reflection diagram, where there is some transmission at all angles of incidence at the same frequency. Figure 6 shows sections of band diagrams for lattices with various scatterer radii, all using the same geometry and boundary conditions as figure 5. The 'flat' mode from figure 5 is drawn as a dashed line. The manner in which the modes develop as a is increased is clearly evident, showing that this is a genuine result, and not a numerical artefact.

Finally, figure 7 shows results for a skewed lattice, with $\mathbf{s}_1 = [1, 0]$, $\mathbf{s}_2 = [0.25, 1]$ and $a = 0.26$. Neumann boundary conditions are in force on the cylinder surfaces. In this case, the irreducible Brillouin zone is the irregular pentagon above the line from $-\mathsf{X}$ to X in figure 2. Despite the fact that the lattice is strongly skewed, the band diagram shows remarkably little asymmetry, particularly at low frequencies. To see this, one must take into account additional symmetries used in producing band diagrams for square lattices. Thus, if $\eta_1 = 0$ then the modes on the line sections $\Gamma\mathsf{X}$ and $\Gamma(-\mathsf{X})$ are symmetric copies, $\overline{\mathsf{M}}\mathsf{M}$ consists of two symmetric copies of the line MX and $-\mathsf{X}\overline{\mathsf{M}}$ is clearly a copy of MX. With this in mind, the similarities between figures 7(a) and 4(a) (where the same parameters are used, except that $\eta_1 = 0$) are clearly evident. On the other hand, the line MN has no analogue in the case of a square lattice, because (7.6) shows that $\mathsf{M} = \mathsf{N}$ if $\eta_1 = 0$. The reflection diagram shown in figure 7(b) appears almost symmetric about $\psi_0 = \pi/2$, but there are significant differences between this and figure 4(b), aside from the distortion caused by asymmetry. In particular, the regimes in which no transmission is possible are smaller, and the three partial band gaps that appear for $7.5 \lessapprox k \lessapprox 9.5$ in figure 4(b) are almost entirely absent from figure 7(b).

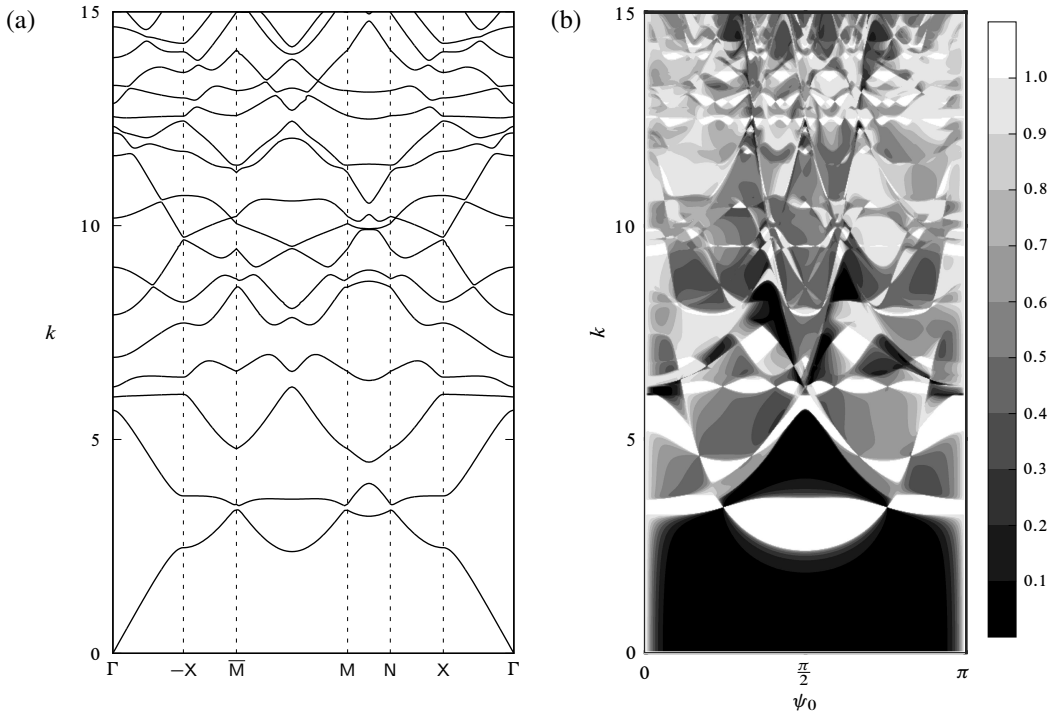

Fig. 7 Band diagram (a) and reflection diagram (b) for a lattice of Neumann scatterers with radius $a = 0.26$ and basis vectors $\mathbf{s}_1 = [1, 0]$, $\mathbf{s}_2 = [0.25, 1]$.

8. Concluding remarks

We have demonstrated that the filtering transformation, which was used in modelling wave interactions with a semi-infinite lattice formed from isotropic point scatterers in (**1**), can also be applied effectively to cases in which the scatterer radius is comparable to the wavelength of the incident field. The complications introduced by this generalisation are relatively minor. The results obtained offer significant insight into wave scattering by periodic structures, particularly at frequencies that lie in pass bands. In particular, given the parameters that describe a wave incident from free space (wavenumber and angle of incidence) it is possible to calculate the proportion of energy that will be converted into Bloch waves and transmitted into the lattice, and the proportion that will be reflected away. This information cannot be gleaned from a standard band diagram, which shows whether modes can pass through a structure, but gives no information about the amplitudes at which these modes are excited by a particular incident field.

The technique could be improved by including slightly damped modes in the filtering process, to further accelerate convergence, and avoid the need to solve large linear systems in cases where modes with small, positive values for $\mathrm{Im}[\beta_y]$ are excited. The method could be also be generalised to other coordinate systems, including spherical polar coordinates for three-dimensional lattice problems. It may be possible to incorporate scatterers of irregular shape via T-matrices (**2**, chapter 7), though how these interact with the filtering transformation requires some investigation. Another possibility relates to the work in (**23**), where it was shown that scattering and reflection effects at the end of

a semi-infinite linear array can be used to predict the effects of wave interactions with long, finite arrays. The same ideas could be applied to structures consisting of large but finite numbers of rows, and have the potential to offer significant savings in computation time.

References

1. I. Thompson and R. I. Brougham. A direct method for Bloch wave excitation by scattering at the edge of a lattice. Part I: point scatterer problem. *Q. J. Mech. Appl. Math.*, 71:1–24, 2018.

2. P. A. Martin. *Multiple Scattering. Interaction of Time-Harmonic Waves with N Obstacles*. Cambridge University Press, 2006.

3. C. M. Linton, R. Porter, and I. Thompson. Scattering by a semi-infinite periodic array and the excitation of surface waves. *SIAM J. Appl. Math.*, 67(5):1233–1258, 2007.

4. J. D. Joannopoulos, S. G. Johnson, J. N. Winn, and R. D. Meade. *Photonic Crystals. Molding the Flow of Light*. Princeton University Press, 2nd edition, 2008.

5. N. Tymis and I. Thompson. Low-frequency scattering by a semi-infinite lattice of cylinders. *Q. J. Mech. Appl. Math.*, 64(2):171–195, 2011.

6. M. Albani and F. Capolino. Wave dynamics by a plane wave on a half-space metamaterial made of plasmonic nanospheres: a discrete Wiener–Hopf formulation. *J. Opt. Soc. Am., B*, 28:2174–2185, 2011.

7. S. G. Haslinger, R. V. Craster, A. B. Movchan, N. V. Movchan, and I. S. Jones. Dynamic interfacial trapping of flexural waves in structured plates. *Proc. Roy. Soc. Lond., A*, 472:20150658 (25 pages), 2016.

8. N. Tymis and I. Thompson. Scattering by a semi-infinite lattice of cylinders and the excitation of Bloch waves. *Q. J. Mech. Appl. Math.*, 67(3):469–503, 2014.

9. N. A. Nicorovici, R. C. McPhedran, and L. C. Botten. Photonic band gaps for arrays of perfectly conducting cylinders. *Phys. Rev. E*, 52(1):1135–1145, 1995.

10. P. McIver. Approximations to wave propagation through doubly-periodic arrays of scatterers. *Waves in Random and Complex Media*, 17(4):439–453, 2007.

11. A. Krynkin and P. McIver. Approximations to wave propagation through a lattice of Dirichlet scatterers. *Waves in Random and Complex Media*, 19(2):347–365, 2009.

12. C. M. Linton. Lattice sums for the Helmholtz equation. *SIAM Review*, 52(4):630–674, 2010.

13. W. J. Parnell and I. D. Abrahams. Multiple point scattering to determine the effective wavenumber and effective material properties of an inhomogeneous slab. *Waves in Random and Complex Media*, 20:678–701, 2010.

14. K. F. Graff. *Wave Motion in Elastic Solids*. Oxford University Press, 1975.

15. C. M. Linton and P. McIver. *Handbook of Mathematical Techniques for Wave/Structure Interactions*. Chapman & Hall/CRC, Boca Raton, 2001.

16. A. Hessel and A. A. Oliner. A new theory of Wood's anomalies on optical gratings. *Applied Optics*, 4(10):1275–1297, 1965.

17. C. M. Linton and I. Thompson. Resonant effects in scattering by periodic arrays. *Wave Motion*, 44:167–175, 2007.

18. L. C. Botten, N. A. Nicorovici, A. A. Asatryan, R. C. McPhedran, C. Martijn de Sterke, and P. A. Robinson. Formulation for electromagnetic scattering and propagation through grating stacks of metallic and dielectric cylinders for photonic crystal calculations. Part II. Properties and implementation. *J. Opt. Soc. Am., A*, 17:2177–2190, 2000.

19. V. Twersky. On the scattering of waves by an infinite grating. *IRE Trans. on Antennas and Propagation*, 4:330–345, 1956.

20. V. Twersky. On scattering of waves by the infinite grating of circular cylinders. *IRE Trans. on Antennas and Propagation*, 10:737–765, 1962.
21. L. C. Botten, N. A. Nicorovici, R. C. McPhedran, C. Martijn de Sterke, and A. A. Asatryan. Photonic band structure calculations using scattering matrices. *Phys. Rev. E*, 64:046603 (18 pages), 2001.
22. I. Thompson and C. M. Linton. Guided surface waves on one- and two-dimensional arrays of spheres. *SIAM J. Appl. Math.*, 70(8):2975–2995, 2010.
23. I. Thompson, C. M. Linton, and R. Porter. A new approximation method for scattering by large finite arrays. *Q. J. Mech. Appl. Math.*, 61(3):333–352, 2008.
24. L. C. Botten, N. A. Nicorovici, A. A. Asatryan, R. C. McPhedran, C. Martijn de Sterke, and P. A. Robinson. Formulation for electromagnetic scattering and propagation through grating stacks of metallic and dielectric cylinders for photonic crystal calculations. Part I. Method. *J. Opt. Soc. Am., A*, 17:2165–2176, 2000.
25. J. Billingham and A. C. King. *Wave Motion*. Cambridge Texts In Applied Mathematics. Cambridge University Press, 2000.
26. J. D. Achenbach. *Wave Propagation in Elastic Solids*. North-Holland, 1973.
27. C. C. Mei, M. Stiassnie, and D. K.-P. Yue. *Theory and Applications of Ocean Surface Waves. Part 1: Linear Aspects*. World Scientific, 2005.
28. D. S. Jones. *The Theory of Electromagnetism*. International Series of Monographs in Pure and Applied Mathematics. Pergamon Press, Oxford, 1964.
29. J. D. Jackson. *Classical Electrodynamics*. John Wiley & Sons, New York, 3rd edition, 1999.

APPENDIX A

Quasiperiodic Green's functions

Spectral representations for the quasiperiodic Green's functions (QPGs) used throughout this paper were derived in detail in (**5**, **8**). Here we repeat only those formulae that are needed in the main text. For a single row of multipoles, the QPG in (2.14) can be expressed in the well-known (**24**, **17**, **8**) form

$$G_n(\mathbf{r};\beta_x) = 2(-\mathrm{i})^{n+1} \sum_{j=-\infty}^{\infty} \frac{\mathrm{e}^{\mathrm{i}\beta_{xj}x-\gamma(\beta_{xj})|y|}}{s_1\gamma(\beta_{xj})} \left[\frac{k}{\beta_{xj}+\gamma(\beta_{xj})}\right]^{n\,\mathrm{sgn}(y)}, \tag{A.1}$$

where β_{xj} and γ are given by (3.2) and (3.3), respectively. The formula (and others derived from it) is not valid on $y = 0$, except in the special case $n = 0$. The QPG for rows $q_0, \ldots, q_1$ is given by

$$\begin{aligned} G_n^{(q_0,q_1)}(\mathbf{r};\boldsymbol{\beta}) &= \sum_{q=q_0}^{q_1} \sum_{j=-\infty}^{\infty} \mathrm{e}^{\mathrm{i}\mathbf{R}_{jq}\cdot\boldsymbol{\beta}} \mathcal{H}_n(\mathbf{r}_{jq}) \\ &= \sum_{q=q_0}^{q_1} \mathrm{e}^{\mathrm{i}q\mathbf{s}_2\cdot\boldsymbol{\beta}} G_n(\mathbf{r}-q\mathbf{s}_2;\beta_x), \end{aligned} \tag{A.2}$$

with $\boldsymbol{\beta} = \beta_x\hat{\mathbf{x}} + \beta_y\hat{\mathbf{y}}$. By using a simple geometric summation to combine contributions from the individual rows, it can be shown that

$$G_n^{(q_0,q_1)}(\mathbf{r};\boldsymbol{\beta}) = 2(-\mathrm{i})^{n+1} \sum_{j=-\infty}^{\infty} \frac{\mathrm{e}^{\mathrm{i}\beta_{xj}x\mp\gamma(\beta_{xj})y}}{s_1\gamma(\beta_{xj})} \left[\frac{k}{\beta_{xj}\pm\gamma(\beta_{xj})}\right]^n \frac{\mathrm{e}^{q_0 w_j^{\pm}} - \mathrm{e}^{(1+q_1)w_j^{\pm}}}{1-\mathrm{e}^{w_j^{\pm}}}, \tag{A.3}$$

where

$$w_j^{\pm} = \pm\eta_2\gamma(\beta_{xj}) + \mathrm{i}(\eta_2\beta_y - 2j\pi\eta_1/s_1). \tag{A.4}$$

The upper and lower signs are to be taken when $y > q_1\eta_2$ and $y < q_0\eta_2$, respectively. For semi-infinite lattices we have

$$G_n^{(q_0,\infty)}(\mathbf{r};\boldsymbol{\beta}) = (-\mathrm{i})^{n+1}\frac{2}{s_1}\sum_{j=-\infty}^{\infty}\frac{\mathrm{e}^{\mathrm{i}\beta_{xj}x+\gamma(\beta_{xj})y}\mathrm{e}^{q_0 w_j^-}}{\gamma(\beta_{xj})(1-\mathrm{e}^{w_j^-})}\left[\frac{k}{\beta_{xj}-\gamma(\beta_{xj})}\right]^n, \quad y < q_0\eta_2 \tag{A.5}$$

and

$$G_n^{(-\infty,q_1)}(\mathbf{r};\boldsymbol{\beta}) = (-\mathrm{i})^{n+1}\frac{2}{s_1}\sum_{j=-\infty}^{\infty}\frac{\mathrm{e}^{\mathrm{i}\beta_{xj}x-\gamma(\beta_{xj})y}\mathrm{e}^{q_1 w_j^+}}{\gamma(\beta_{xj})(1-\mathrm{e}^{-w_j^+})}\left[\frac{k}{\beta_{xj}+\gamma(\beta_{xj})}\right]^n, \quad y > q_1\eta_2. \tag{A.6}$$

The full lattice Green's function, $G_n^{(-\infty,\infty)}(\mathbf{r};\boldsymbol{\beta})$ can be obtained by setting $q_0 = q_1 + 1$ and adding (A.5) to (A.6). Note that $G_n^{(-\infty,\infty)}(\mathbf{r};\boldsymbol{\beta})$ has the two-dimensional quasiperiodicity property (4.1).

The expansions (A.1), (A.5) and (A.6) all appear when the reflected and transmitted fields are calculated, in which case $\beta_x = k\cos\psi_0$, and β_{xj} is expressed in terms of scattering angles using (6.2). Some further simplifications are then possible. For the single row Green's function, we find that

$$G_n(\mathbf{r};k\cos\psi_0) = \frac{2(-\mathrm{i})^n}{ks_1}\sum_{j=-\infty}^{\infty}\mathrm{e}^{\mathrm{i}k(x\cos\psi_j+|y|\sin\psi_j)}\,\frac{\mathrm{e}^{\mathrm{i}n\,\mathrm{sgn}(y)\psi_j}}{\sin\psi_j}. \tag{A.7}$$

For multiple rows, we begin by using the fact that $2j\pi/s_1 = k(\cos\psi_j - \cos\psi_0)$ in (A.4) to obtain

$$\mathrm{e}^{w_j^+} = \rho_j\mathrm{e}^{\mathrm{i}\mathbf{s}_2\cdot\boldsymbol{\beta}} \quad \text{and} \quad \mathrm{e}^{w_j^-} = \tau_j^{-1}\mathrm{e}^{\mathrm{i}\mathbf{s}_2\cdot\boldsymbol{\beta}}, \tag{A.8}$$

where

$$\rho_j = \mathrm{e}^{-\mathrm{i}k(\eta_1\cos\psi_j+\eta_2\sin\psi_j)} \quad \text{and} \quad \tau_j = \mathrm{e}^{\mathrm{i}k(\eta_1\cos\psi_j-\eta_2\sin\psi_j)}. \tag{A.9}$$

After substituting these into (A.5) and (A.6), we find that

$$G_n^{(q_0,\infty)}(\mathbf{r};\boldsymbol{\beta}) = \frac{2(-\mathrm{i})^n}{ks_1}\,\mathrm{e}^{\mathrm{i}q_0\mathbf{s}_2\cdot\boldsymbol{\beta}}\sum_{j=-\infty}^{\infty}\frac{\mathrm{e}^{\mathrm{i}k(x\cos\psi_j-y\sin\psi_j)}\mathrm{e}^{-\mathrm{i}n\psi_j}}{\tau_j^{q_0}(1-\tau_j^{-1}\mathrm{e}^{\mathrm{i}\mathbf{s}_2\cdot\boldsymbol{\beta}})\sin\psi_j}, \quad y < q_0\eta_2 \tag{A.10}$$

and

$$G_n^{(-\infty,q_1)}(\mathbf{r};\boldsymbol{\beta}) = \frac{2(-\mathrm{i})^n}{ks_1}\,\mathrm{e}^{\mathrm{i}q_1\mathbf{s}_2\cdot\boldsymbol{\beta}}\sum_{j=-\infty}^{\infty}\frac{\mathrm{e}^{\mathrm{i}k(x\cos\psi_j+y\sin\psi_j)}\rho_j^{q_1}\mathrm{e}^{\mathrm{i}n\psi_j}}{(1-\rho_j^{-1}\mathrm{e}^{-\mathrm{i}\mathbf{s}_2\cdot\boldsymbol{\beta}})\sin\psi_j}, \quad y > q_1\eta_2. \tag{A.11}$$

APPENDIX B

Energy flux

In the preceding sections, the integral (3.6) is used in two slightly different ways. In deriving a conservation of energy condition (see §6), $\mathcal{S}$ is taken to be a parallelogram, and it is always the case that $\langle E_{\mathcal{S}}\rangle = 0$. Since $\mathcal{S}$ is a closed contour, this result can be derived immediately by applying Green's second identity to the total field and its complex conjugate. In applying the radiation condition (see §4), $\mathcal{S}$ is taken to be a straight line and (3.6) is used to determine the direction in which Bloch waves transport energy across this line. The argument which shows that this is valid is presented for one possible formulation in acoustics in (**5**). Here we give brief derivations for acoustics, electromagnetism, elasticity and water wave theory. Some general points are worth noting beforehand. First, for two time-harmonic functions

$$F(\mathbf{r};t) = \mathrm{Re}\big[f(\mathbf{r})\mathrm{e}^{-\mathrm{i}\omega t}\big] \quad \text{and} \quad G(\mathbf{r};t) = \mathrm{Re}\big[g(\mathbf{r})\mathrm{e}^{-\mathrm{i}\omega t}\big], \tag{B.1}$$

the time-average over one period is given by

$$\big\langle FG\big\rangle = \frac{\omega}{2\pi}\int_0^{2\pi/\omega} F(\mathbf{r};t)G(\mathbf{r};t)\,\mathrm{d}t = \frac{1}{2}\,\mathrm{Re}\big[f(\mathbf{r})g^*(\mathbf{r})\big]. \tag{B.2}$$

Here, the integral has been evaluated using the identity $2\,\mathrm{Re}[z_1]\,\mathrm{Re}[z_2] = \mathrm{Re}[z_1 z_2] + \mathrm{Re}[z_1 z_2^*]$, though of course one can simply proceed by writing out the real components of $f(\mathbf{r})\mathrm{e}^{-\mathrm{i}\omega t}$ and $g(\mathbf{r})\mathrm{e}^{-\mathrm{i}\omega t}$. The second point concerns dimensions. Initially, we will integrate over an appropriately chosen area $\mathcal{A}$. The means by which this can be reduced to a line integral then depend on the relationship between two-dimensional problems and the underlying three-dimensional physics. Since taking the time-average does not affect dimensions, we should expect to integrate a quantity with dimensions of mass per time cubed over $\mathcal{A}$ to obtain the rate of energy transport across $\mathcal{A}$. Finally, we note that the direction of Bloch wave propagation is often determined using the group velocity vector, which in our notation is given by

$$\nabla_{\boldsymbol{\beta}}\omega = \left[\frac{\partial\omega}{\partial\beta_x}, \frac{\partial\omega}{\partial\beta_y}\right] \tag{B.3}$$

(see (**4**, pp.40–42), for example). The relationship between group velocity and energy flux is discussed in the appendix to (**21**). Energy flux is used in this article because ω and $\boldsymbol{\beta}$ are related by the linear system (4.11), and evaluating the partial derivatives in (B.3) is not straightforward. On the other hand, once the Bloch vector $\boldsymbol{\beta}$ and corresponding coefficients B_n have been computed, all coefficients in the expressions for energy flux are determined explicitly.

B.1 *Acoustic waves*

This is the simplest case. The necessary physics is described in (**25**, §§3.1–3.3). The acoustic intensity (the rate of working of the pressure fluctuation) is given by

$$\mathbf{I} = P\mathbf{V}, \tag{B.4}$$

where P is the pressure fluctuation and $\mathbf{V}$ is the fluid velocity. Introducing the acoustic potential U, we have

$$\mathbf{V} = \nabla U \quad \text{and} \quad P = -\rho\frac{\partial U}{\partial t}, \tag{B.5}$$

where ρ is the quiescent fluid density. Therefore, from (B.4),

$$\mathbf{I} = -\rho\frac{\partial U}{\partial t}\nabla U, \tag{B.6}$$

and the rate of energy transport across $\mathcal{A}$ is given by the surface integral

$$E_{\mathcal{A}} = -\rho\int_{\mathcal{A}} \frac{\partial U}{\partial t}\,\hat{\mathbf{n}}\cdot\nabla U\,\mathrm{d}\mathbf{s}, \tag{B.7}$$

where $\hat{\mathbf{n}}$ is a unit vector perpendicular to $\mathcal{A}$. If we now assume time-harmonic motion as in (2.20) and take the average using (B.2) with $F = \partial U/\partial t$ and $G = \hat{\mathbf{n}}\cdot\nabla U$, we obtain

$$\langle E_{\mathcal{A}}\rangle = \frac{\rho\omega}{2}\int_{\mathcal{A}} \mathrm{Re}\left[\mathrm{i}u(\mathbf{r})\frac{\partial}{\partial n}u^*(\mathbf{r})\right]\mathrm{d}\mathbf{s} \tag{B.8}$$

$$= -\frac{\rho\omega}{2}\,\mathrm{Im}\int_{\mathcal{A}} u(\mathbf{r})\frac{\partial}{\partial n}u^*(\mathbf{r})\,\mathrm{d}\mathbf{s}. \tag{B.9}$$

Here, $\partial/\partial n$ indicates differentiation in the direction of the normal $\hat{\mathbf{n}}$. If $\langle E_{\mathcal{A}}\rangle > 0$ then the net rate of energy transport across $\mathcal{A}$ is in the same direction. Had we used a pressure formulation, then

$$P(\mathbf{r};t) = \mathrm{Re}\big[p(\mathbf{r})\mathrm{e}^{-\mathrm{i}\omega t}\big], \tag{B.10}$$

and it follows from (B.5) that $p = \mathrm{i}\omega\rho u$. In this case, (B.9) becomes

$$\langle E_{\mathcal{A}}\rangle = -\frac{1}{2\rho\omega}\,\mathrm{Im}\int_{\mathcal{A}} p(\mathbf{r})\frac{\partial}{\partial n}p^*(\mathbf{r})\,\mathrm{d}\mathbf{s}. \tag{B.11}$$

Two-dimensional acoustic problems are generally obtained by assuming no variation in a certain direction, z, say. The surface integral in (B.9) (or (B.11)) can then be replaced by a line integral over a curve $\mathcal{S}$ perpendicular to the z axis, and $\langle E_{\mathcal{S}}\rangle$ represents the net rate of energy transport across $\mathcal{S}$ per unit length in z.

B.2 *Elastic waves*

In component notation, the instantaneous rate of work of the traction in direction i is given by (**26**, section 1.3)

$$\mathcal{P}_i = -\tau_{ij}\frac{\partial U_j}{\partial t}, \tag{B.12}$$

where the stress tensor τ_{ij} for a homogeneous isotropic solid is given by (**26**, eqn (2.28)). For a time-harmonic SH problem, with no variation in the z (3) direction, we have $U_1 = U_2 = 0$, and so (B.12) simplifies to

$$\mathcal{P}_i = -\mu\frac{\partial U}{\partial x_i}\,\frac{\partial U}{\partial t}, \tag{B.13}$$

where $U = U_3$, $i = 1$ or 2 and μ is a Lamé constant. The rate of working in the direction of $\hat{\mathbf{n}}$ is therefore

$$\mathcal{P}_n = -\mu\,\hat{\mathbf{n}}\cdot\nabla U\,\frac{\partial U}{\partial t}. \tag{B.14}$$

This is exactly the same as the potential formulation in the acoustic case, but with the Lamé constant in place of the density. Consequently, for time-harmonic motion with u given by (2.20),

$$\langle E_{\mathcal{A}}\rangle = -\frac{\mu\omega}{2}\,\mathrm{Im}\int_{\mathcal{A}} u(\mathbf{r})\frac{\partial}{\partial n}u^*(\mathbf{r})\,\mathrm{d}\mathbf{s}. \tag{B.15}$$

B.3 *Water waves*

The case of linear water waves in fluid of constant depth h is also similar to a potential formulation in acoustics. The only significant difference occurs due to the relationship between two- and three-dimensional problems. Thus, if U is the velocity potential, then the rate of working of the hydrodynamic force is $-\rho\partial U/\partial t\,\nabla U$, i.e. the dynamic pressure multiplied by the particle velocity (**15**, chapter 1) (see also (**27**, chapter 1)). It then follows immediately that $E_{\mathcal{A}}$ is again given by (B.7), but now with u related to the physical velocity potential via (2.21). If $\mathcal{A}$ is a surface that extends uniformly throughout the fluid depth (e.g. a rectangle or a cylinder), then, in place of (B.9) we obtain

$$\langle E_{\mathcal{A}}\rangle = -\frac{\rho\omega}{2}\int_{-h}^{0}|\phi_0(z)|^2\,\mathrm{d}z\;\mathrm{Im}\int_{\mathcal{S}} u(\mathbf{r})\frac{\partial}{\partial n}u^*(\mathbf{r})\,\mathrm{d}s, \tag{B.16}$$

where $\mathcal{S}$ is a cross section of $\mathcal{A}$ with z fixed.

B.4 *Electromagnetic waves*

The Poynting vector, which represents instantaneous power flow due to the electric and magnetic fields is given by (**28**, sections 1.25 & 1.28)

$$\mathbf{P} = \mathbf{E}\times\mathbf{H}. \tag{B.17}$$

A multiplicative factor of $c/(4\pi)$ appears in some formulations; this is due to the use of Gaussian, rather than SI, units (see table 3 in appendix 2 of (**29**)). Assuming the time-harmonic form

$$\mathbf{E} = \mathrm{Re}[\mathbf{e}\,\mathrm{e}^{-\mathrm{i}\omega t}] \quad\text{and}\quad \mathbf{H} = \mathrm{Re}[\mathbf{h}\,\mathrm{e}^{-\mathrm{i}\omega t}] \tag{B.18}$$

and observing that each element of $\mathbf{E}\times\mathbf{H}$ is a linear combination of products, each formed from one element from $\mathbf{E}$ and one from $\mathbf{H}$, we see that the generalisation of (B.2) to the electromagnetic case is

$$\big\langle\mathbf{E}\times\mathbf{H}\big\rangle = \frac{1}{2}\,\mathrm{Re}\big[\mathbf{e}\times\mathbf{h}^*\big]. \tag{B.19}$$

The time-averaged energy flux across an area $\mathcal{A}$ is therefore given by

$$\langle E_{\mathcal{A}}\rangle = \frac{1}{2}\,\mathrm{Re}\int_{\mathcal{A}}\hat{\mathbf{n}}\cdot(\mathbf{e}\times\mathbf{h}^*)\,\mathrm{d}\mathbf{s}. \tag{B.20}$$

Subsequently we will use the convention that there is no implied conjugation of operands in complex vector products. This choice does not affect (B.20) (since the real part is taken on the right-hand side), but the convention must be applied consistently in order to reach the correct result. As in acoustics, two-dimensional electromagnetic problems are generally obtained by assuming no variation in a particular direction, z, say. For the particular case of TE waves, we have $\mathbf{h} = u(\mathbf{r})\,\hat{\mathbf{z}}$, where u satisfies the Helmholtz equation. We then use the fact that

$$\nabla \times \mathbf{H} = \epsilon_0 \frac{\partial \mathbf{E}}{\partial t}, \tag{B.21}$$

where ϵ_0 is the electric permittivity of the exterior medium, to obtain

$$\mathbf{e} = \frac{\mathrm{i}}{\epsilon_0 \omega} \nabla \times \mathbf{h}. \tag{B.22}$$

By using this to eliminate $\mathbf{e}$ from (B.20), we find that the time-averaged energy flux per unit length in z is given by the line integral

$$\langle E_{\mathcal{S}} \rangle = -\frac{1}{2\epsilon_0 \omega} \operatorname{Im} \int_{\mathcal{S}} \hat{\mathbf{n}} \cdot \big((\nabla \times \mathbf{h}) \times \mathbf{h}^* \big) \,\mathrm{d}s, \tag{B.23}$$

where $\mathcal{S}$ is a cross section of $\mathcal{A}$ with z fixed. Writing out the components of the triple vector product now yields

$$\langle E_{\mathcal{S}} \rangle = -\frac{1}{2\epsilon_0 \omega} \operatorname{Im} \int_{\mathcal{S}} \hat{\mathbf{n}} \cdot \left(\left[\frac{\partial}{\partial y} u(\mathbf{r}),\ -\frac{\partial}{\partial x} u(\mathbf{r}), 0 \right] \times \mathbf{h}^* \right) \mathrm{d}s \tag{B.24}$$

$$= -\frac{1}{2\epsilon_0 \omega} \operatorname{Im} \int_{\mathcal{S}} u(\mathbf{r}) \frac{\partial}{\partial n} u^*(\mathbf{r}) \,\mathrm{d}s. \tag{B.25}$$

Finally, for TM waves, we have $\mathbf{e} = u(\mathbf{r})\,\hat{\mathbf{z}}$ and

$$\nabla \times \mathbf{E} = -\mu_0 \frac{\partial \mathbf{H}}{\partial t}, \tag{B.26}$$

where μ_0 represents magnetic permeability. After eliminating $\mathbf{h}$ from (B.20), we proceed as in the TE case, and we find that

$$\langle E_{\mathcal{S}} \rangle = -\frac{1}{2\omega \mu_0} \operatorname{Im} \int_{\mathcal{S}} u(\mathbf{r}) \frac{\partial}{\partial n} u^*(\mathbf{r}) \,\mathrm{d}s. \tag{B.27}$$